Lawrence Berkeley National Laboratory

Title

Biofouling of filtration membranes in wastewater reuse: In situ visualization with confocal laser scanning microscopy

Permalink

https://escholarship.org/uc/item/4qp3n44z

Authors

Tow, Emily W
Rad, Behzad
Kostecki, Robert

Peer reviewed

Biofouling of filtration membranes in wastewater reuse: in situ visualization with confocal laser scanning microscopy

Emily W. Tow[a,b,*], Behzad Rad[c], Robert Kostecki[a,*]

[a]*Energy Storage and Distributed Resources Division, Lawrence Berkeley National Laboratory, 1 Cyclotron Rd., Berkeley, California, USA*
[b]*F. W. Olin College of Engineering, 1000 Olin Way, Needham, Massachusetts, USA*
[c]*Molecular Foundry, Lawrence Berkeley National Laboratory, 67 Cyclotron Rd., Berkeley, California, USA*

Abstract

The filtration membranes utilized in advanced treatment of municipal wastewater are prone to biological fouling. Permeability loss and water recovery limitations due to fouling necessitate additional pretreatment and membrane cleaning, which raise the cost of water reuse. Better fouling mitigation calls for a deeper understanding of biofilm behavior on water reuse membranes. This study uses confocal microscopy to monitor biofouling under realistic conditions. To simulate water reuse, a miniature flow cell with microfiltration and ultrafiltration membranes was operated under typical filtration conditions using secondary effluent from California's East Bay Municipal Utility District. The growing biofilms were stained for extracellular polymeric substances and live and dead cells, and they were monitored in situ under filtration conditions with a confocal laser scanning microscope to produce 2-D and 3-D images. In situ image series revealed biofilm growth and removal processes including internal and external fouling, extracellular polymeric substance production, wrinkling, delamination, and film re-deposition. Additionally, changes in biofilm morphology between in situ and ex situ images highlighted limitations of ex situ imaging. These results provide insight into the physical and biological mechanisms of biofouling in hopes of informing the development of improved techniques for biofouling mitigation.

Keywords: water reuse, membrane fouling, confocal laser scanning microscopy, ultrafiltration, microfiltration

1. Introduction

While membrane-based potable reuse of municipal wastewater is rapidly expanding as

a low-energy method of mitigating water scarcity [1], membrane fouling remains a common

*Address correspondence to *etow@olin.edu* and *r_kostecki@lbl.gov*.

concern. In water reuse facilities, membrane fouling raises water cost by necessitating extensive pretreatment and frequent membrane cleaning as well as limiting water recovery [2]. Membrane fouling occurs due to the buildup of various constituents including microbes, dissolved organic and inorganic species, and suspended solids on the membranes through which water permeates [3, 4]. Biological fouling (biofouling) is particularly problematic in water reuse due to the relatively high microbial count and organic content of municipal wastewater [5]. Fouling can be mitigated to some extent through feed water pretreatment and specialized membrane coatings, and can also be partially or fully reversed by cleaning the membrane with detergents, acidic or alkaline solutions, chelating agents, or biocides [6], but the limited efficacy of current techniques drives further research in fouling prevention. Better understanding of the interplay between the biology and transport phenomena that dictate biofilm formation [7] and the mechanics that influence biofilm removal has the potential to inform the development of improved fouling mitigation techniques.

Visualization of fouling behaviors under relevant filtration conditions has the potential to inform the design of innovative fouling mitigation strategies. For example, a novel method of chemical-free, deformation-induced cleaning [8] of organic-fouled reverse osmosis (RO) membranes derived inspiration from in situ observation of alginate fouling delamination [9]. Optical coherence tomography (OCT) has been used to create in situ videos and time-lapse image series of the fouling layer in plane view and in cross section to better understand biofouling of UF membranes [10, 11, 12]. Epifluorescence microscopy was used with a high-pressure RO membrane flow cell to visualize the spatial distribution of bacterial deposition and understand the influence of feed spacers on RO membrane biofouling [13]. Other nondestructive optical techniques for biofouling characterization include two-photon femtosecond imaging [14] and optical microscopy [15], both of which have been used with yeast. Such visualization studies complement quantitative studies using metrics such as permeate flux decline and longitudinal pressure drop, which have enabled comparisons of biofouling rates

between different operating conditions (e.g., temperature [16]) and processes (e.g., RO vs. forward osmosis (FO) [17]). Together, quantitative measurements and visualization techniques enable researchers to better understand, predict, and mitigate biofouling.

Confocal laser scanning microscopy (CLSM) enables visualization of the composition and morphology of biofilms [18, 19], and it has occasionally been used in situ to observe biofilm growth as it occurs. CLSM provides a 3-D view of biofilm morphology, which can be complex and hard to predict or measure [20], and the various labeling methods available allow for visualization of biofilm composition and morphology together, especially when CLSM is combined with other microscopy techniques [21, 22]. For example, activated sludge supernatant biofilms formed on a glass slide were examined with both CLSM and Raman microscopy [23] to determine the change in EPS composition over a period of three months. Fluorescent labeling of extracellular polymeric substances (EPS), which serve a host of purposes in biofilms [24], and other biofilm constituents, such as proteins and cells, enables CLSM to reveal biofilm structure and behavior. Klausen et al. [25] used in situ CLSM to create high-resolution, time-lapse 3-D images of the mushroom-shaped structures formed by *Pseudomonas aeruginosa* on glass and determine the effect of cell motility on biofilm conformation. Their study tagged mutated and unmutated cells with different fluorescent proteins to avoid photobleaching and stain cytotoxicity, which pose challenges to long-term CLSM imaging of live cells. Due to its ability to differentiate species and strains, the fluorescent in situ hybridization (FISH) method of fluorescence-tagging particular DNA or RNA sequences has been particularly successful in enabling CLSM to elucidate the structure and dynamics of multispecies biofilms [26, 27]. In addition to providing qualitative visualization of biofilm behavior, analysis of 3-D CLSM images allows for quantification of biofilm volume and spatial distribution of biofilm constituents [28].

CLSM has been used ex situ to examine the structure and composition of biofilms formed on water treatment membranes, specifically, to complement macroscopic fouling metrics such

3

as flux decline. For example, Farias et al. [29] collected ex situ CLSM images of biofouling of RO membranes treating membrane bioreactor effluent to reveal changes in biofilm morphology and composition over time. Kwan et al. [17] visualized biofilm conformation ex situ on RO and forward osmosis (FO) membranes and found that the harvested FO biofilms were thicker and more heterogeneous in shape than those grown in RO, which enabled interpretation of the mechanisms for the slower flux decline typically observed in FO.

Although CLSM has previously been used in situ for non-membrane biofilms (e.g., in Ref. [25]), permeation through a membrane has significant effects on biofilm thickness and shape [30], and thus it is important to study membrane biofouling under permeation conditions. Bar Zeev et al. [31] examined the effect of a subtle change in sample preparation for ex situ biofilm imaging—the addition of a glass coverslip—and found significant changes in biofilm conformation occurred. Ex situ visualization of biofilm morphology, while capable of high resolution, is limiting because removal from the environment in which the biofilm was grown has the potential to cause conformational changes. However, to our knowledge, biofilms grown under permeation conditions have only been imaged with CLSM ex situ due to the challenge of imaging pressurized liquids with optical microscopy.

In this study, CLSM was used to visualize biofouling of water treatment membranes in situ and *operando*, i.e., under conditions of permeation and cross-flow. Biofouling in microfiltration (MF) and ultrafiltration (UF)—key filtration processes in water reuse that typically precede RO [2]—were simulated using a transparent, pressurizable, miniature flow cell outfitted with an MF or UF membrane. Secondary effluent from a municipal wastewater treatment plant was filtered through the flow cell under cross-flow and flux conditions typical of water reuse facilities, including frequent membrane backwashes. This novel method of in situ CLSM imaging of membrane biofouling under permeation conditions allows for visualization of hydrodynamic and biological mechanisms of biofouling. We hope these images will enhance understanding of biofouling behavior and inform the development of future

4

biofouling mitigation strategies for water reuse.

2. Methods

In this study, the MF/UF step in municipal wastewater reuse was simulated using a custom-designed flow cell. Secondary municipal wastewater effluent was circulated through a transparent, pressurizable cross-flow filtration cell designed for in situ optical probing with CLSM.
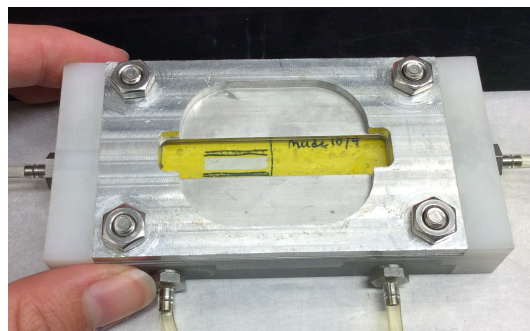
2.1. Apparatus

The experimental apparatus, which is depicted in Fig. 1, allowed for pressurized filtration of municipal wastewater effluent through MF and UF membranes under conditions typical of wastewater reuse while allowing for in situ visualization of membrane fouling. A custom flow cell (Fig. 1b) was designed to hold a membrane between a feed channel containing a feed spacer (Sterlitech 31 mil diamond), which enabled backwashing of the flat sheet membrane, and a permeate channel containing a permeate carrier cut from a commercial spiral-wound RO membrane (Membrane Solutions).

The cell was designed to incorporate a standard 1 mm-thick, 1"×3" (approximately 25×75 mm) glass or quartz microscope slide; quartz was used in this study for its superior shatter resistance. In preliminary tests, quartz slides in the experimental apparatus withstood 3–6 barg of pressure before shattering, which was sufficient to operate filtration through MF and UF membranes, and the 1 mm slide was thin enough to allow biofilm visualization with long working distance objectives. The small opening in the metal plate above the slide, the plastic sheet between the slide and the plate, and the O-ring grooves were designed to minimize stress concentration on the slide. However, despite careful design and the use of a pressure relief valve in the flow loop, the slide occasionally cracked during long experiments, requiring cleaning the apparatus and starting the trial over from the be-

5
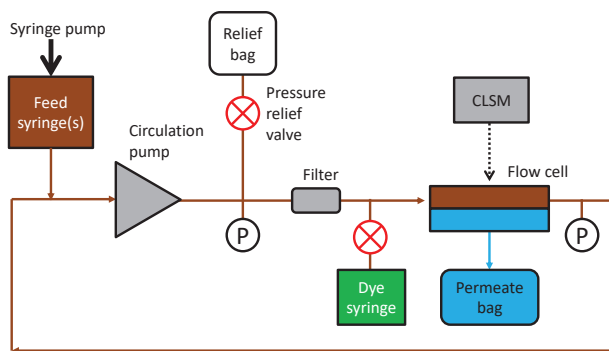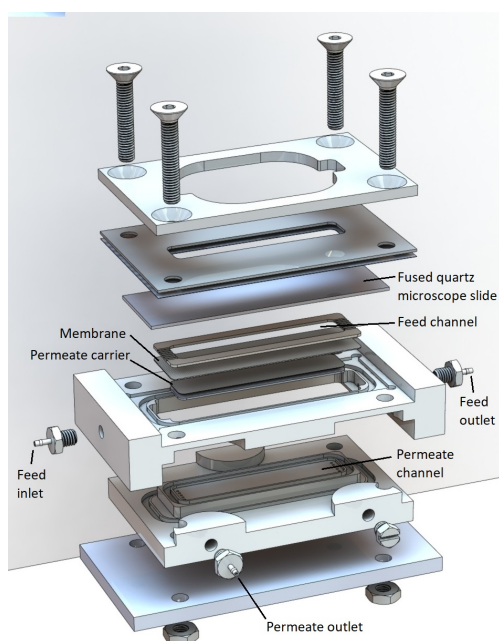
Figure 1: Experimental apparatus: (a) schematic diagram of flow system, where P represents a pressure gauge and a crossed circles represents a valve; (b) photograph of the flow cell; (c) exploded view of flow cell design (sealing O-rings not pictured).

ginning. Researchers wishing to replicate or adapt the flow cell used in this work may do so by downloading the SolidWorks files provided in the Supplementary Information.

Permeate flux was controlled by a syringe pump (New Era Pump), which injected liquid into a fluidic system of approximately constant volume (with some variation due to tubing flexibility and pressure changes), so that the flow rate through the membrane was approxi-

mately equal to the syringe pump flow rate. Backwashing was conducted by programming the syringe pump to periodically withdraw liquid from the flow loop, thus pulling permeate back through the membrane into the feed.

Cross-flow velocity in the flow cell was set by a magnetic-drive circulation pump (Ismatec drive with Micropump head) that was calibrated with a rotameter before fouling tests. A 25 µm filter was installed in the flow loop to catch pieces of biofilm removed from the membrane during the backwash step, since these would be swept away during the backwash step in a real treatment facility.

The flow system was cleaned and disinfected between trials by flushing effluent out with water; disassembling the flow cell and scrubbing parts with soap and water; flushing the reassembled system with ethanol; flushing the ethanol out with tap water; and, finally, flushing the tap water out with deionized water.

2.2. Membranes

Commercial membranes were used for both filtration processes. The UF membrane was a polyethersulfone (PES) 10 kDa molecular weight cutoff (MWCO) Microdyn Nadir UF membrane. The MF membrane was a polyvinylidene fluoride (PVDF) membrane from Synder (V0.1) with a nominal pore size of 0.1 µm. SEM images of both membranes are provided in Appendix C. Although hollow fiber MF and UF membranes are more common in practice than flat sheet membranes [2], flat sheet membranes were used in this study to enable plane views of fouling accumulation and removal processes.

To define the active area and prepare membranes for use in the miniature flow cell, membrane coupons were first laid between sheets of 0.001" (0.025 mm) adhesive-backed polyimide film, from which rectangles had been removed, in order to provide a smooth surface against which the flow cell's O-ring could form a seal. Nail polish, an adhesive commonly used to seal microscope slides, was carefully applied to the edges of the rectangular cutout on the active surface of the membranes to prevent permeation through any defects that might

7

have been introduced at the contact line between the membrane and the adhesive film. The region of the active layer not covered with adhesive film or nail polish was considered the active area for calculating permeate flux. All membranes were prepared with active areas of approximately 0.25 cm^2 to enable visualization of several regions between spacer filaments; active areas for calculating flux were calculated from microscope images.

Before installing in the flow cell, UF membranes were dipped in 1:1 ethanol:water solution for approximately 10 s to wet the support layer and enhance permeability before rinsing with deionized water and installing in the flow cell; MF membranes were only rinsed with deionized water.

2.3. Wastewater effluent

Several samples of secondary wastewater effluent prior to disinfection were obtained from clarifier outflow at the East Bay Municipal Utility District (EBMUD) wastewater treatment plant in Oakland, California, USA. Samples were stored at 4±1 °C and used within five weeks of collection. Wastewater composition was characterized by CalTest Labs (USA; Table 1). Cell counts on Luria broth agar plates after 48 hours at room temperature found the cell count to range from about 5,000–30,000 CFU/ml, a fluctuation which is similar in magnitude to the seasonal fluctuations seen in plate counts of other treatment plants [32]. However, Ref. [32] found that the typical cell count by flow cytometry was 3–4 orders of magnitude higher than plate counts due to the difficulty of growing wastewater effluent bacteria on plates, so it is likely that the density of cells in the wastewater effluent was higher than determined by plate counts. It is likely that the wastewater microbial composition changed both between samples taken in different seasons and between collection and testing, which we acknowledge is a limitation of this study.

Table 1: Wastewater effluent composition at approximately one week of sample age

Characteristic	Value
pH	7.2
Total dissolved solids (TDS) (mg/L)	970
Total suspended solids (TSS) (mg/L)	<2
Total nitrogen (mg/L)	72
Nitrate and nitrite (mg/L)	<0.07
Dissolved organic carbon (DOC) (mg/L)	20
Biological oxygen demand (BOD) (5-day) (mg/L)	7
Phosphorus (mg/L)	6.0

2.4. Fouling and cleaning

Operating conditions were chosen to mimic realistic MF/UF operation to the extent possible in the miniature flow cell. MF and UF were operated at average fluxes (during permeate production) of 300 and 80 LMH, respectively, except where noted, and with a feed flow rate chosen to create a cross-flow velocity of 25 cm/s.

When backwashes were employed, both membrane types were operated with backwash cycles every 45 min for 2.25 min at equal and opposite flux as the permeate production step to simulate an overall backwash-limited recovery ratio of 90%, which is within the typical range of 90–95% [33]. Each trial with backwash continued for long enough for a clear and consistent fouling pattern to develop (2–4 days); new room-temperature wastewater was added each day. Additional trials were conducted for shorter times to elucidate fouling behavior in the absence of backwashing.

2.5. Staining

Stains were selected to differentiate live cells from dead, highlight EPS, and be distinguishable by CLSM. DAPI (4',6-diamidino-2-phenylindole) or Hoechst 33342 (referred to as Hoechst in the following) are cell-permeable live cell stains that were used (individually) to dye all cells; propidium iodide (PI), which is not cell-permeable, was used to stain dead

9

cells only. Wheat germ agglutinin–Alexa Fluor 555 conjugate (referred to as WGA in the following) was chosen as a stain to highlight EPS because it adheres to N-acetylglucosamine and sialic acid [34] and was found to highlight EPS in a wide range of bacterial biofilms by Neu and Kuhlicke [35]. However, because EPS includes a wide range of polysaccharides and proteins that are not all bound by WGA, WGA cannot highlight all EPS. Due to the limitation of selecting a few stains that are distinguishable by CLSM and the common desire to additionally stain cell DNA, fluorescence-based biofilm imaging studies often choose a single lectin to stain glycoconjugates of EPS and stand in for an EPS stain (e.g., *Aleuria aurantia* in Ref. [28]). In the present study, WGA was chosen as a sole lectin to capture the general shape of EPS accumulation at scales larger than the optical resolution of the present imaging method (several µm). Although EPS will be used as shorthand for the parts of the biofilm highlighted by fluorescence-tagged WGA in the remainder of this paper, it is possible for there to be additional EPS that is not bound by WGA and thus not visualized.

Approximately 1 h before imaging, concentrated dyes (1 mg/mL for Hoechst, WGA, and PI and 1-14 mM for DAPI) were added to approximately 0.5 mL of deionized water and injected slowly into the flow loop upstream of the flow cell. Live cell dyes were sometimes used throughout the duration of experiments and sometimes applied only at the end in order to determine whether dye toxicity affected fouling behavior; as discussed in Appendix A, no marked differences were seen. Stain concentrations stated in the results section (on the order of µg/mL) are based on an estimated feed loop volume of 17 mL; concentration of stains in the biofilm may be greater due to permeation of stains through the biofilm as water flows through the membrane. Stain concentrations and contact times were chosen through preliminary experimentation to find the lowest concentrations that would allow for clear imaging and the lowest contact time (about 30 min) that would allow for equilibration of image brightness. Final (post-dilution) concentrations were within the ranges recommended for individual stains in their respective manuals [36, 37, 38, 34]; the chosen wait time of 30

10

min met or exceeded recommended minimum incubation times for all stains. The 30-min wait time also allowed for adequate mixing of injected stains with the wastewater effluent by circulation more than 200 times through the flow loop.

Because injection occurred upstream of the flow cell while filtration was occurring, the stained biofilm formed through two mechanisms: The existing biofilm was stained as convection and diffusion brought unattached stain molecules to the biofilm, and also water constituents (unattached microbes, carbohydrates, etc.) may have been stained and then assembled into a biofilm. Any water constituents that were stained and that did not form the biofilm either passed through the membrane (and thus were not imaged) or stayed in the bulk solution, where their concentration was low enough compared to the biofilm to not meaningfully affect the images. The concentration of dissolved organic carbon (a lower bound on the concentration of organic water constituents) in the wastewater effluent was 20 mg/L (Table 1), whereas the stains were an order of magnitude lower in final concentration (typically 1-3 mg/L), so stains should not have significantly interfered with the buildup of water constituents into a biofilm. That said, the potential for interference of stains with biofilm formation is a possible limitation of staining-based in situ imaging, as discussed in Sec. 3.5.3.

The membranes used in this study were largely permeable to the stains, with one exception. Although the MF membrane's nominal pore size of 0.1 μm far exceeds the size of all four stains, allowing unattached stain molecules to pass through so as not to affect the biofilm images, the stains adhered to the clean MF membranes somewhat, as seen in CLSM images (e.g., in Fig. A.20) at the beginning of fouling trials. The 10 kDa UF membrane's pores are large enough to pass PI (at 668 Da), DAPI (at 277 Da), and Hoechst 33342 (at 453 Da), but not WGA (at 38 kDa), so it is possible for WGA to build up on the UF membrane independently of the biofilm, as will be discussed in Sec. 3.4. However, 3-D views of UF fouling do not show disproportionate accumulation of WGA on the membrane surface (see,

11

e.g., Fig. 10).

2.6. Confocal imaging

Confocal imaging was conducted using a Zeiss LSM710 confocal laser scanning micro-scope. 405 nm and 561 nm lasers were used to excite DAPI/Hoechst and PI/Alexa Fluor 555, respectively. Emission detector ranges were selected using ZEN 2011's dye spectrum database and built-in optimization[1]. The thickness of the fluid channel and enclosing glass required the use of long-working-distance objective lenses. A 10x objective (10x Plan-Neofluar 0.30 NA, Carl Zeiss) was used with a pinhole corresponding to one Airy unit for the lowest wavelength imaged in all trials except where noted. A 50x long working distance objective (50x Epiplan Neofluar 0.55 NA/DIC, Carl Zeiss) was also used in some trials, but clearer images were typically obtained with the 10x objective, digital magnification of 5x, and a slow imaging speed, the combination of which allowed for visualization of some individual cells. All confocal images included in this study were captured in situ and *operando* (i.e., with the membrane in place in the flow cell and with permeation and cross-flow) unless otherwise noted. Coordinates of imaged regions were recorded relative to the corner of the membrane active area to enable repeated imaging of the same region.

Image collection and initial processing were conducted with ZEN 2011 (Zeiss). Channel intensities were normalized consistently within each series of images. When estimating biofilm volume from 3-D stacks, ImageJ was used with a thresholding procedure similar to that of Staudt et al. [28]: a single threshold was set manually for what minimum intensity in the WGA channel indicated the presence of biofilm in a time series of 3-D images, and product of the number of voxels above the threshold intensity and the voxel volume gave

---

[1]Detector ranges varied depending on the set of dyes used as follows: 410–509 nm for Hoechst or DAPI (regardless of other dyes used); 550–579 nm for Alexa Fluor 555 when used with Hoechst and PI; 540–579 nm for Alexa Fluor 555 when used with DAPI and PI; 545–578 nm for Alexa Fluor 555 when used with PI only; 623–719 nm for PI when used with Alexa Fluor 555 and Hoechst or DAPI; and 623–685 nm for PI when used with Alexa Fluor 555 only.

an estimate of the total biofilm volume on the region of membrane imaged. Dividing by the imaged area allowed for calculation of average thickness. However, significant staining of the MF membrane prevented the calculation of biofilm volume in MF because the membrane and biofilm could not be distinguished by intensity alone.

In each imaging session, a tiled image was collected of the entire fouled region of each membrane, and higher-resolution images (some in 3-D) were collected at several locations that were consistent throughout a given fouling trial (see Fig. 3 for an example). With this combination of images at each time step, we hoped to capture a range of fouling behaviors at different scales. More images were collected than are presented in this report; the images shared here were selected with the intention to represent and illustrate features seen throughout the larger set of images.

3. Results and discussion

The images collected in this study show the progression of biofouling on MF and UF membranes through in situ visualization of simulated water reuse with real wastewater effluent. Although periodic backwashing of porous membranes is integral to fouling mitigation in real water reuse facilities, fouling observation is conducted both with and without backwash (as described in Sec. 2.4) to elucidate phenomena that occur between and in the absence of backwash cycles.

3.1. Microfiltration without backwash

MF of wastewater effluent was conducted for 8 h at 300 LMH flux without backwash to determine baseline MF fouling behavior. Stains were added with the effluent to reach concentrations of 1.8 µg/mL each of Hoechst and PI and 2.9 µg/mL WGA. Half the initial amount of dye was added before collecting images at 4 h and 8 h.

Figure 2 shows the progression of the biofilm in one region, including magnified images of the region's center, over the 8 h period. Live and dead cells (in blue and red, respectively)

are visible in the magnified images (Fig. 2 d, and f). In Figs. 2a and b, the membrane is shown before significant biofilm deposition, highlighting the membrane's large (50 µm-scale) internal pores just below the membrane surface, which appear in the CLSM images and are also visible in SEM images of the clean MF membrane (Fig. C.25b). Due to convection of material to the membrane, a flat biofilm containing live cells, dead cells, and EPS develops over much of the membrane surface. Tiled images of the entire active area (collected but not included here) show similar behavior across the membrane.

The magnified images (Fig. 2 d, and f) show an accumulation of live cells around the edges of larger internal pores. Cell accumulation in large pores was confirmed in SEM images of fouled MF membranes (Fig. C.24d). The enhanced image brightness near the pore edge may be due to the steepness of the pore there and thus the large number of live cells seen by the long working distance objective, which has poor vertical resolution. The surface biofilm is less bright above the fouled internal pores, perhaps indicating a difference in external biofouling behavior where internal biofouling occurs.

3.2. Microfiltration with backwash

MF was conducted with wastewater effluent for 4 d at 300 LMH with backwashes every 45 min (as described in Section 2.4) to determine fouling behavior under the influence of periodic backwashing. Before imaging, dye was added to reach concentrations of 1.8 µg/mL each of Hoechst and PI and 2.9 µg/mL WGA. As explained in Appendix A, a similar test was conducted separately without Hoechst for comparison because of the effects of Hoechst on cell reproduction [39]; qualitatively, results were similar with and without daily application of Hoechst.

Figure 3a shows the entire fouled membrane after 1 d as well as several close-up images. Initially, the MF biofilm builds up in a relatively flat layer with some internal fouling, as observed in MF without backwashing, but two new features emerge: a striped pattern occurs parallel to the expected direction of flow and a few small cracks appear in the biofilm. Later,
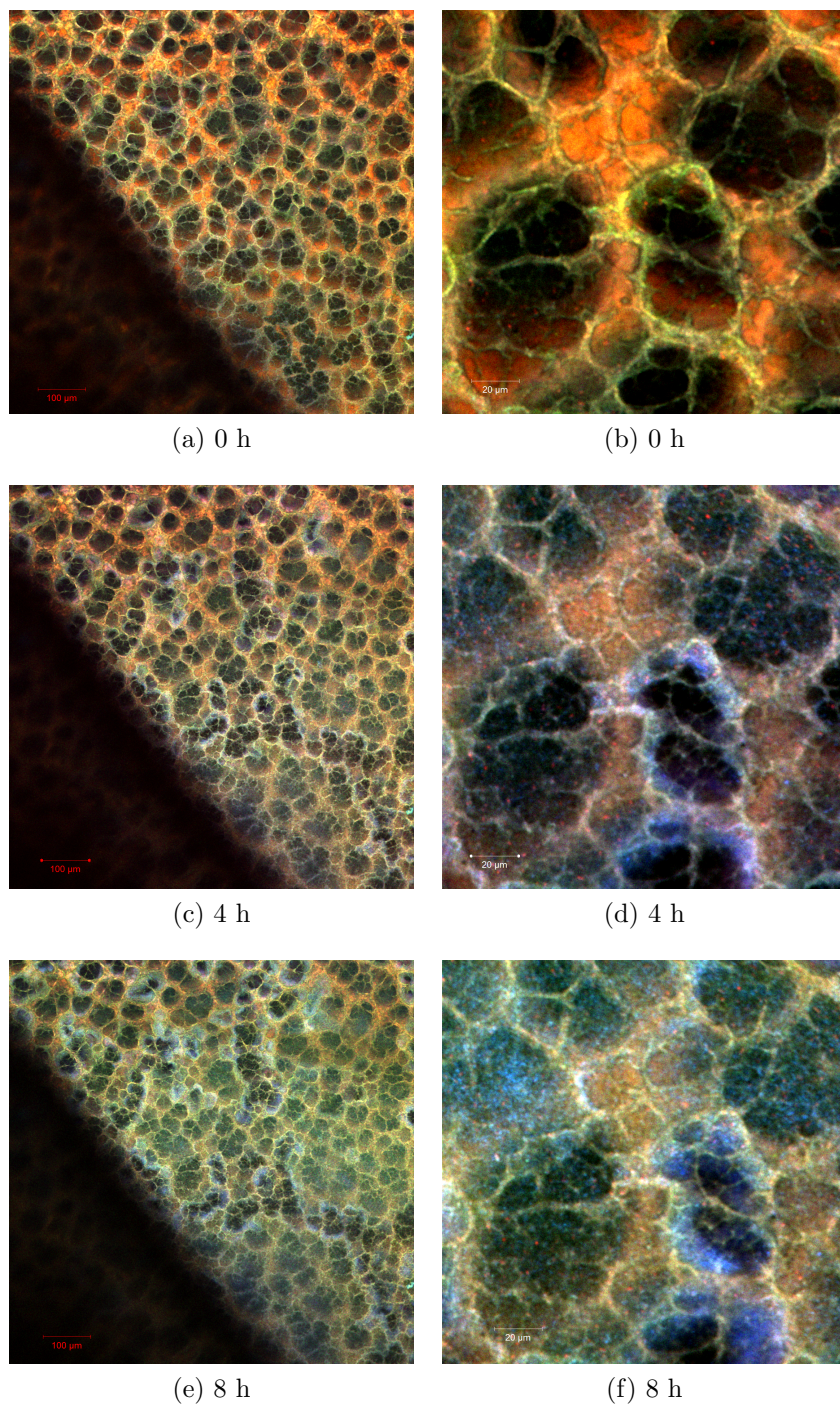
14

Figure 2: Confocal images of a region of MF membrane after different durations of fouling without backwash. (b), (d), and (f) are magnified images collected at the center of (a), (c), and (e), respectively. Blue = cells (Hoechst); green = EPS (WGA); red = dead cells (PI).
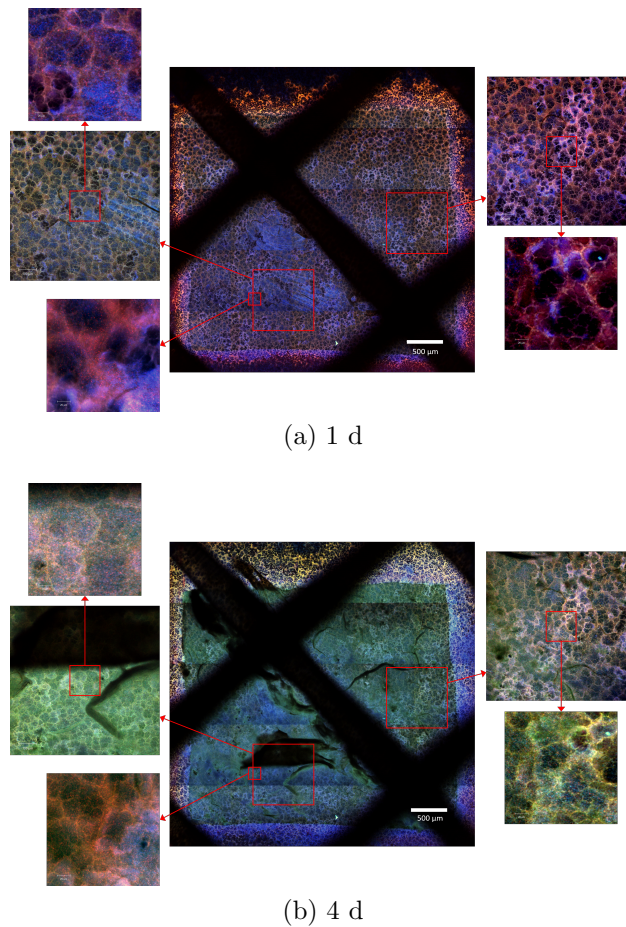
(a) 1 d

(b) 4 d

Figure 3: Tiled confocal images of fouled MF membrane after (a) 1 d and (b) 4 d of fouling with higher-resolution images taken at several locations. Blue = cells (Hoechst); green = EPS (WGA); red = dead cells (PI). Cross-flow was from right to left; dark diagonal lines are spacer filaments. Apparent horizontal stripes in the tiled images are an artefact of tiling.

two 3-D structures appear: large wrinkles, which appear as dark, curved lines; and flaps, which appear as large dark patches. These structures are visible in Fig. 3b, which shows the membrane after 4 d of fouling. These structures may appear dark due to extending above the confocal plane. The flaps are concentrated downstream of the spacer filament that lays flat on the membrane (the diagonal line from upper left to lower right) in arcs, which may indicate peeling in the direction of flow from the line of contact between the spacer and the membrane. Both flaps and wrinkles grow and move over time. The remainder of the biofilm remains relatively flat; refer to Fig. 17a for a 3-D image of a section of this biofilm after 4 d.

Dark spots—both holes in the biofilm and small domes where the film appears to be locally detached from the membrane—also occur, and are more visible in cross-section (Fig. 17a). Holes and wrinkles in the biofilm are also visible in SEM images of fouled MF membranes (Fig. C.24a,c).

Magnified images of the MF biofilm (Fig. 4) reveal stages of biofilm growth above and below the active layer. Individual dead cells (red specks) are visible, appearing primarily on the upper surface of the membrane, particularly in regions between large internal pores. Live cells (in blue) congregate in the vicinity of several internal pores, densely populating the rightmost pore over time and leaving a dark hole in the middle. EPS (green) is less obvious in Fig. 4, but the color shift over time from red to orange on the membrane surface and blue to turquoise in the open pore indicates EPS buildup over time both on the membrane surface and in the internal pore.

Figure 5 separates the image of the fouled MF membrane at 4 d (Fig. 4d) into individual detector channels, corresponding to individual dyes, to more clearly show the distribution of biofilm constituents on the membrane. Live cells (i.e., specks of light that appear in Fig. 5a but not Fig. 5b) can be seen congregating in the lower right, while dead cells are spread more evenly over the membrane. Dead cells appear brighter in Fig. 5b (the PI channel) than Fig. 5a (the Hoechst channel) due to the use of minimal levels of the cell-permeable stain Hoechst. EPS appears cloudy relative to the cells, and is brighter where there are more live cells. The ratio between total cells and dead cells in the internal pore, which appears light blue in the lower-right portion of Fig. 4, is shown to be higher than that on the membrane surface by the intensity profiles shown in Fig. 5d, suggesting the occurrence of cell proliferation within the pore.

The apparent internal fouling of the MF membrane shown in Figs. 2, 4, and 5 is confirmed by CLSM images of the edges of MF membranes, 3-D CLSM scans, and ex situ SEM images. At the edges of the active membrane area, which were sealed as described in Section 2.2,
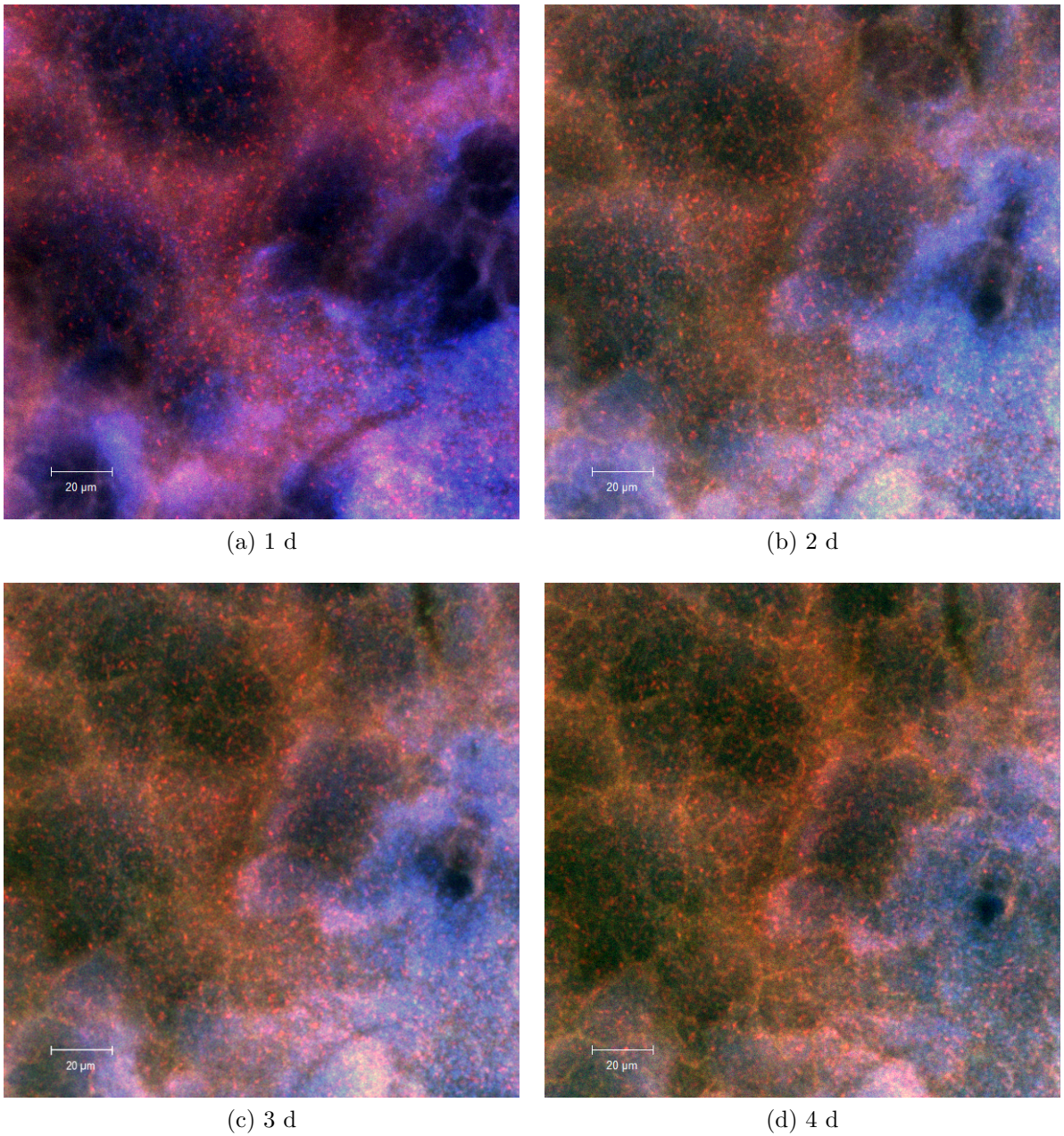
17

Figure 4: High-resolution confocal images of fouled MF membrane shown in Fig. 3, collected after 1–4 d of fouling with 50x objective. Blue = cells (Hoechst); green = EPS (WGA); red = dead cells (PI).

EPS can be seen accumulating beneath the sealed surface along the edges of networks of large pores beneath the active layer in Fig. 6. The biofilm appears to grow easily within a given network of connected internal pores, perhaps beginning with a large-enough hole in the
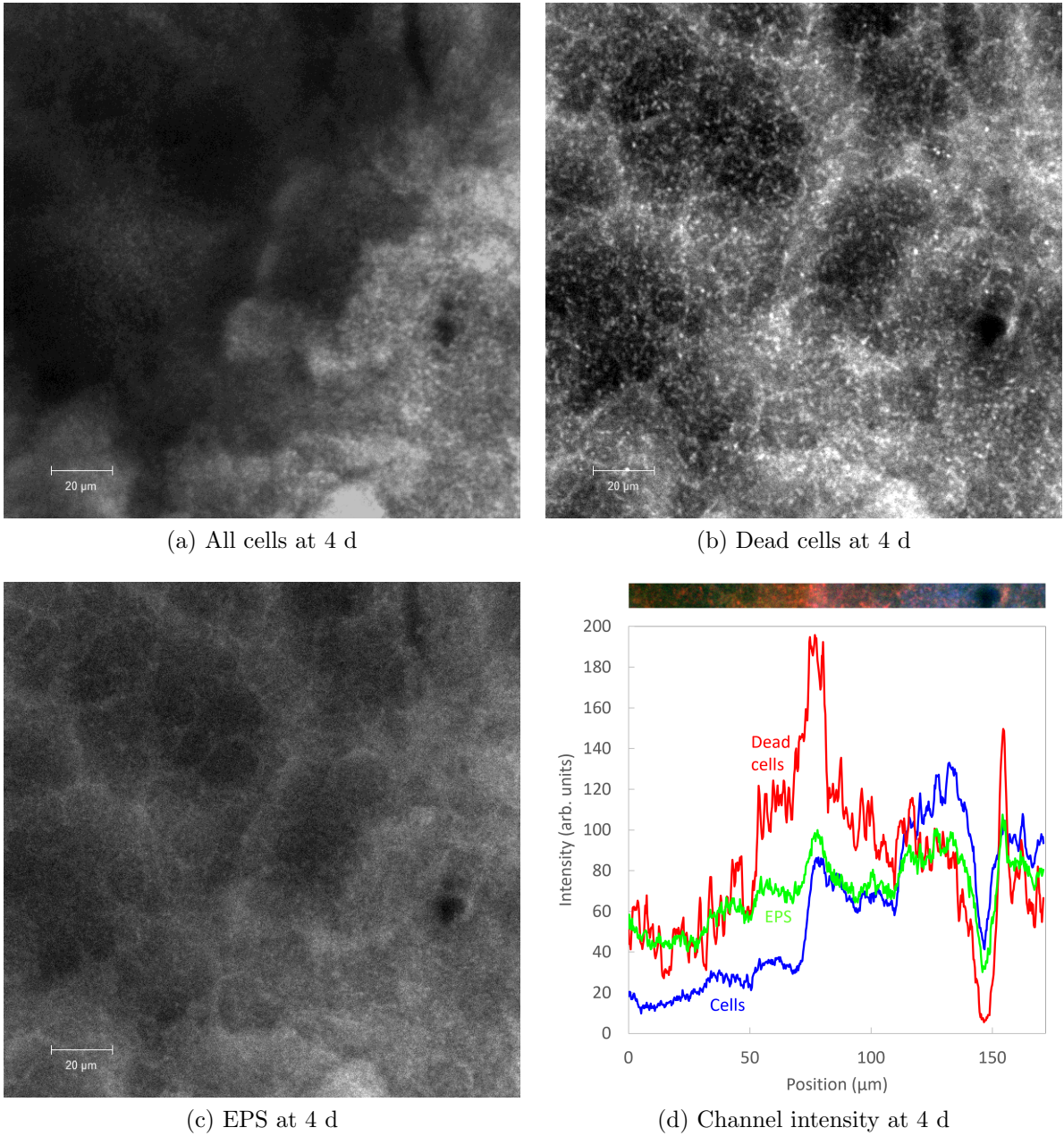
(a) All cells at 4 d

(b) Dead cells at 4 d

(c) EPS at 4 d

(d) Channel intensity at 4 d

Figure 5: (a–c) The fouled MF membrane of Fig. 4d (at 4 d of age) visualized using separate detector channels for each dye to show the distribution of biofilm constituents. (d) Plot of intensity at 4 d along the horizontal region of Fig. 4d shown above the plot, which intersects the dark spot seen in the micrographs.

unsealed membrane surface for bacteria to pass through; such holes are shown in an SEM image of an unfouled MF membrane (Fig. C.25a). Bacteria are also seen lining these large internal pores in ex situ SEM images (Fig. C.24d) and a 3-D CLSM image (Fig. 7, below) of

19

the same fouled membrane imaged by SEM, in which cells and EPS can be seen extending below the surface of the membrane within some relatively large internal pores. These images demonstrate that internal biofouling, which is difficult to remove through backwashing, can be significant in MF.
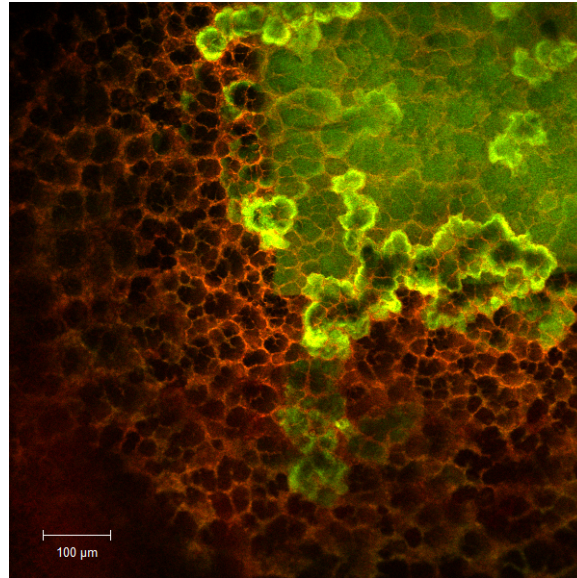
Figure 6: Internal fouling under top-sealed edges of active MF membrane region. This membrane was fouled for 3 days without Hoechst as described in Appendix A. Green = EPS (WGA); red = dead cells (PI).

The efficacy of backwashing in cleaning this MF membrane was limited. A separate experiment was conducted to visualize the membrane before and after backwashing, with results shown in Fig. 8. Comparing the before and after images, this particular backwash cycle was ineffective at removing both internal and external fouling; one flap of biofilm in the middle of the frame moved slightly, but the film largely stayed attached, with several flaps peeling away from the membrane in the direction of flow. This result highlights the cohesiveness of biofilms and the difficulty of removing a biofilm adhered to a flat sheet membrane. This result also highlights a limitation of the experimental backwashing procedure: it did not include air scouring, which would typically accompany backwash in water reuse facilities [33].
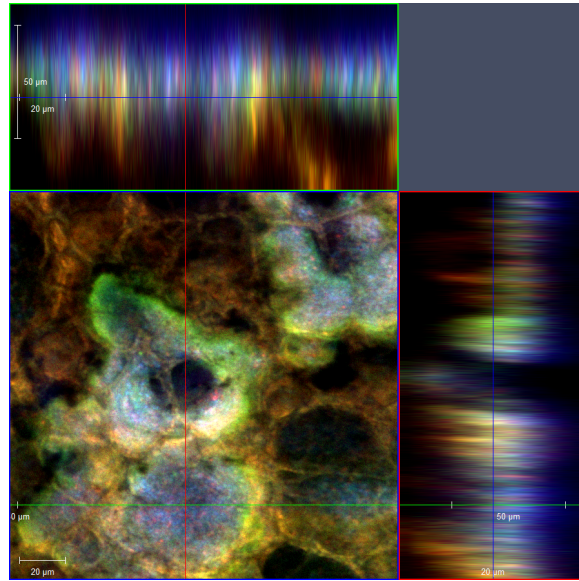
Figure 7: CLSM image showing internal and external fouling in MF. Blue = cells (Hoechst); green = EPS (WGA); red = dead cells (PI).
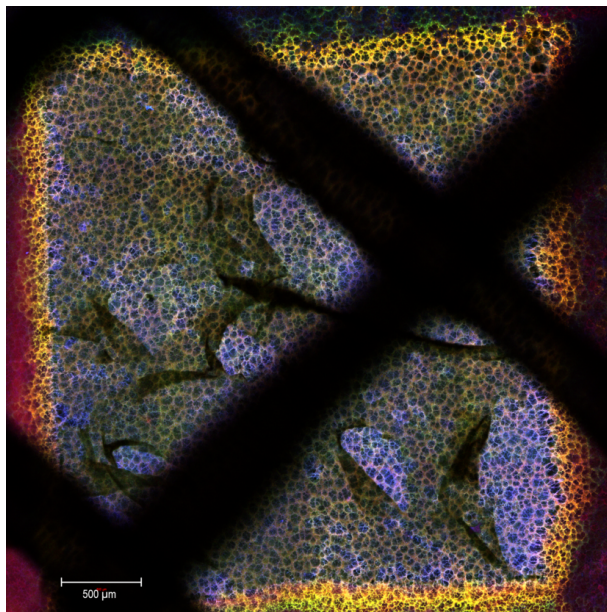
(a) Before backwash
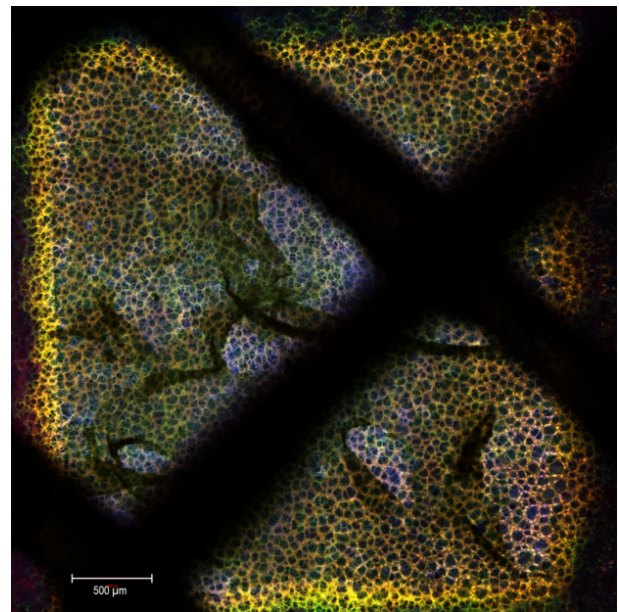
(b) After backwash

Figure 8: Confocal images of 2-day fouled MF membrane before and after a backwash. Blue = cells (Hoechst); green = EPS (WGA); red = dead cells (PI).

3.3. Ultrafiltration without backwash

To visualize baseline biofouling behavior in UF, wastewater effluent was stained with 2.4 µg/mL WGA, 2.4 µM DAPI, and 4.7 µg/mL PI, and was filtered through a UF membrane at a flux of 48 LMH with a cross-flow velocity of 20 cm/s. During one hour of filtration, pressure increased from 1.1 to 2.1 bar, indicating significant fouling. CLSM images of the membrane were collected in situ during filtration.

Figure 9 shows a tiled scan of the entire active area using a 10x objective. The fouled membrane exhibited curved stripes of both cells and EPS as well as patches of black dots, likely representing holes or channels through the biofilm. Figure 10 shows 3-D cross-sections of a primarily striped region of the biofilm. Stripes and holes appear in a regular pattern between consecutive cells of the spacer, with stripes appearing approximately tangential to the expected direction of flow. The holes congregate near spacer filaments and on the concave sides of the striped arcs.
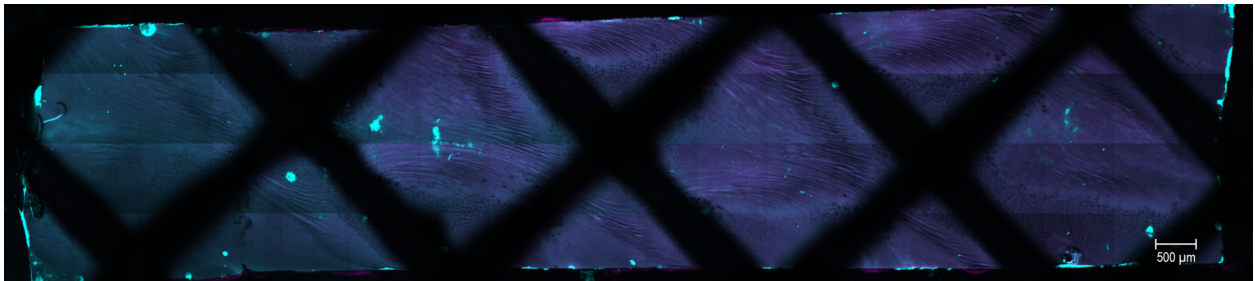
Figure 9: UF membrane fouled for approximately one hour during cross-flow from right to left. Cyan = DAPI; magenta = EPS (WGA); the combination appears purple. Readers may zoom in to see details of fouling pattern.

Other in situ membrane biofouling visualization studies with comparable feed spacers have revealed somewhat similar macroscopic fouling patterns despite differences in imaging methods, hydrodynamics, and membranes. In an in situ optical coherence tomographic study of biofouling on unpressurized NF membranes with the same type of spacer, Fortunato et al. [12] saw membrane fouling concentrated upstream of each spacer filament that was
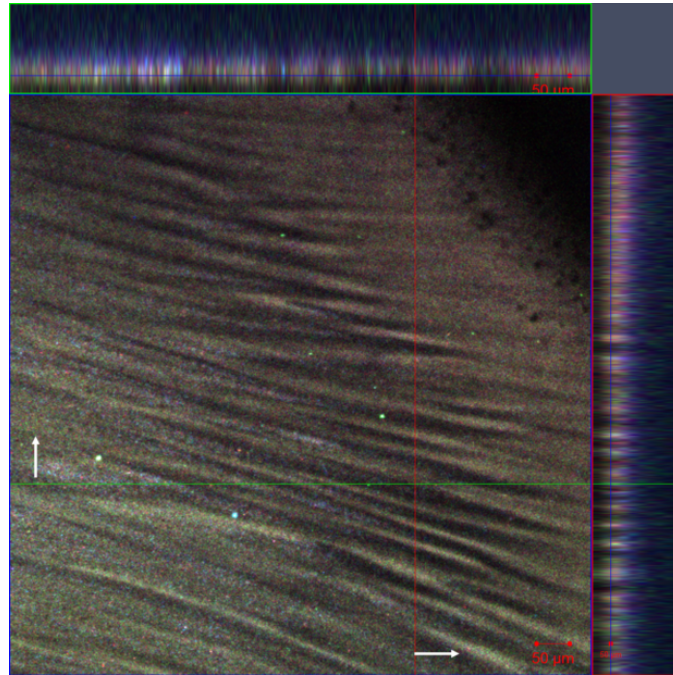
22

Figure 10: Depth section of stripe and spot patterns from the fouled membrane of Fig. 9. Cyan = cells (DAPI); green = EPS (WGA); red = dead cells (PI). Depth section planes are indicated with arrows.

farther from the membrane. Perhaps due to the significant flux through the UF membrane in the present study and the association between higher permeate flux and increased spatial uniformity [30], the biofilm is distributed more uniformly over the membrane; however, there is heterogeneity in patterning within each cell of the spacer. The region upstream of each elevated spacer filament that showed the most membrane fouling in Fortunato et al. is the region of the UF membrane in Figs. 9 and 10 that has the least patterning (neither pronounced stripes nor pits). Similarly, the downstream corner of each spacer cell (which is the left corner of each cell in Fig. 9) had the highest bacterial load in forward osmosis biofouling in a study by Kastl et al. [30]. In contrast, however, Huang et al. [13] found the fastest accumulation of bacteria on an RO membrane to be in the upstream corner of each feed spacer cell, although the spacer did not fill the entire feed channel in that study. Stripes and holes were not visible in any past in situ visualization studies of filtration membrane biofouling known to the authors. Given that the pattern of stripes and spots observed in Fig.

9 is repeated in the spaces between each set of spacer filaments, the lines and spots likely represent self-organization of the microbes and other constituents that make up the biofilm, rather than a pattern related to membrane structure or surface heterogeneity. A similar pattern of stripes was recorded after 1 d of MF fouling (Fig. 3a). Patterned morphologies such as these may help the biofilm survive in local hydrodynamic conditions, as discussed below.

Patterns of holes in biofilms, as seen in Figs. 9 and 10, have been noted when biofilms disperse. McDougald et al. [40] review mechanisms of biofilm dispersal, which often involves EPS degradation, cell lysis, and dispersal of a select few bacteria, leaving a hollow micro-colony. Increase or rapid decrease in nutrient concentration or depletion of oxygen can lead to dispersal. The biofilm forming *P. aeruginosa* is known to form hollow microcolonies prior to dispersal of cells [41]. Similar round channels through the biofilm have been observed with CLSM on *P. aeruginosa*-fouled RO membranes after cleaning by osmotic backwashing [42].

Various rough patterns occur in biofilms when nutrient scarcity leads to unstable growth. Stewart [43] reviewed effects of convection on biofilm formation, emphasizing how increased mass transfer at peaks in a rough biofilm structure leads to increased local growth rates, creating an instability resulting in increasingly rough biofilms. For example, *P. aerugi-nosa* biofilms grown under oxygen-depleted conditions [44] developed stripes. The stripes and possibly also the holes observed in the present study's biofilms may results from the improvement in nutrient capture enabled by biofilm roughness under convection conditions.

3.4. Ultrafiltration with backwash

The in situ CLSM images in this section show how fouling progressed on the UF membrane over four days of operation with periodic backwashing. Before imaging, dyes were added to each a final dilution of 0.6 µg/mL of WGA and PI and 0.6 µM DAPI. After the first day of fouling at 54 LMH, limited fouling was observed, and flux was increased to 80

24

LMH. Over the 4 d fouling period, operating pressure increased by a factor of two, indicating significant fouling. Foulant accumulation was heterogeneous on a range of scales. By the third day, Fig. 11 shows that an overall pattern develops: large flakes of EPS-rich material stick to the membrane, while some areas are nearly clean, particularly after backwashing. Some of the EPS-rich regions appear to be composed of multiple layers of folded or wrinkled flakes. A very large flake, which could be seen flapping in the flow through the microscope eyepiece, appears as a dark, diagonal blur in the left-hand side of Figs. 12a and 12b. Some small regions of the membrane appear to perpetually remain clean.
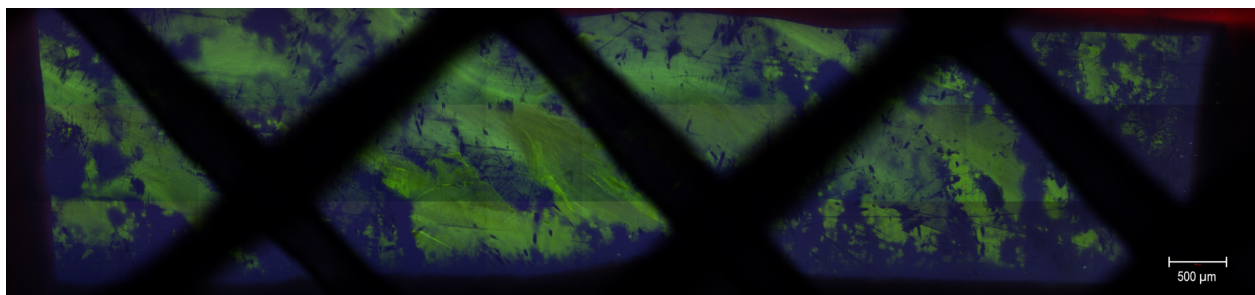
(a) Before backwash
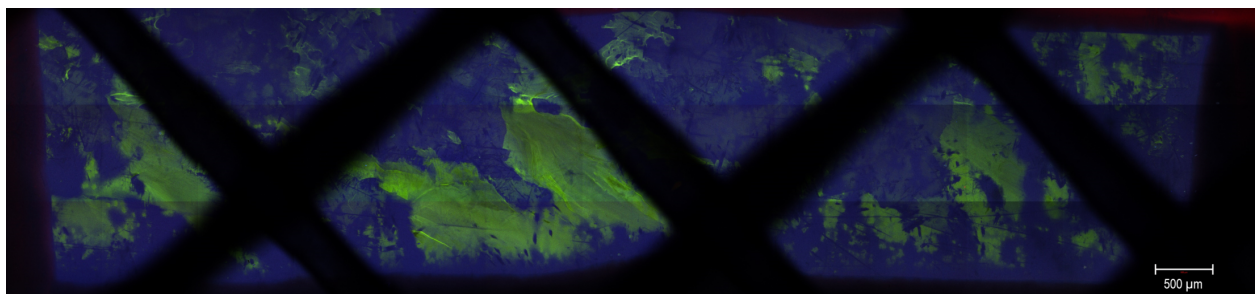
(b) After backwash

Figure 11: Tiled confocal images of 2 day-old UF biofilm captured in situ before and after a backwash. Flow was right to left. Blue = DAPI; green = EPS (WGA); red = dead cells (PI)..

The accumulation process between backwash cycles is illustrated in Fig. 13, showing three accumulation behaviors: (1) small regions (order 10 µm in width) remain dark throughout the permeate production step, indicating low local membrane permeability; (2) most of the membrane is relatively clean of EPS right after a backwash, but gradually accumulates

25
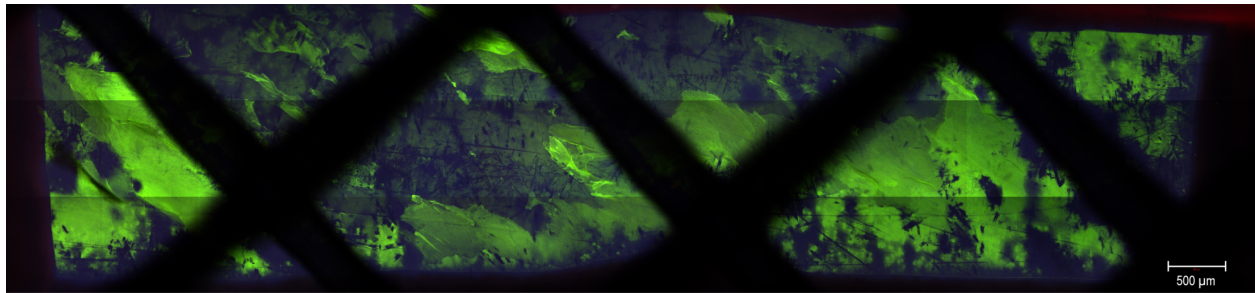
(a) 3 d
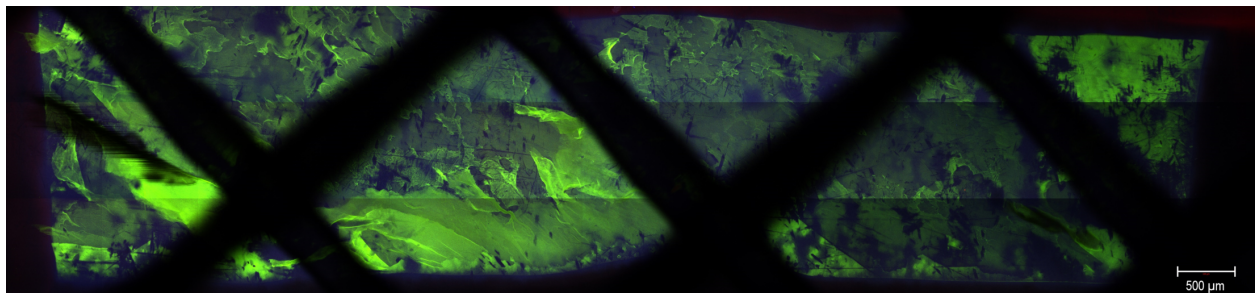
(b) 4 d

Figure 12: Confocal images of UF biofilm captured in situ after (a) 3 d and (b) 4 d. Flow was right to left. Blue = DAPI; green = EPS (WGA); red = dead cells (PI).

foulant (possibly including fluorescent but unbound WGA lectins) over the course of permeate production; and (3) regions of membrane that were not cleaned by the backwash step are already so thickly fouled that local permeation is lower and further foulant accumulation during permeation is limited. In regions exhibiting the second behavior (periodic fouling and cleaning), a lacy pattern of dark spots in the WGA-rich material develops beginning on the third day (see Figs. 14c,e and the upper-right corner of Figs. 14a,c) that is most evident later in each permeate production cycle (see Fig. 13). These spots (likely holes in the biofilm, as discussed in Section 3.3) are similar in size to those seen on the UF membrane without backwash (Figs. 9 and 10). Stripes and wrinkles in the direction of flow, as discussed in Section 3.3, persist, but appear more subtle with periodic backwash than without.

The progression of fouling on the UF membrane is substantially shaped by the effects of backwashing. Comparison of Figs. 11a and 11b shows that backwashing removes biofouling

(a) Before backwash

(b) 4 min after backwash
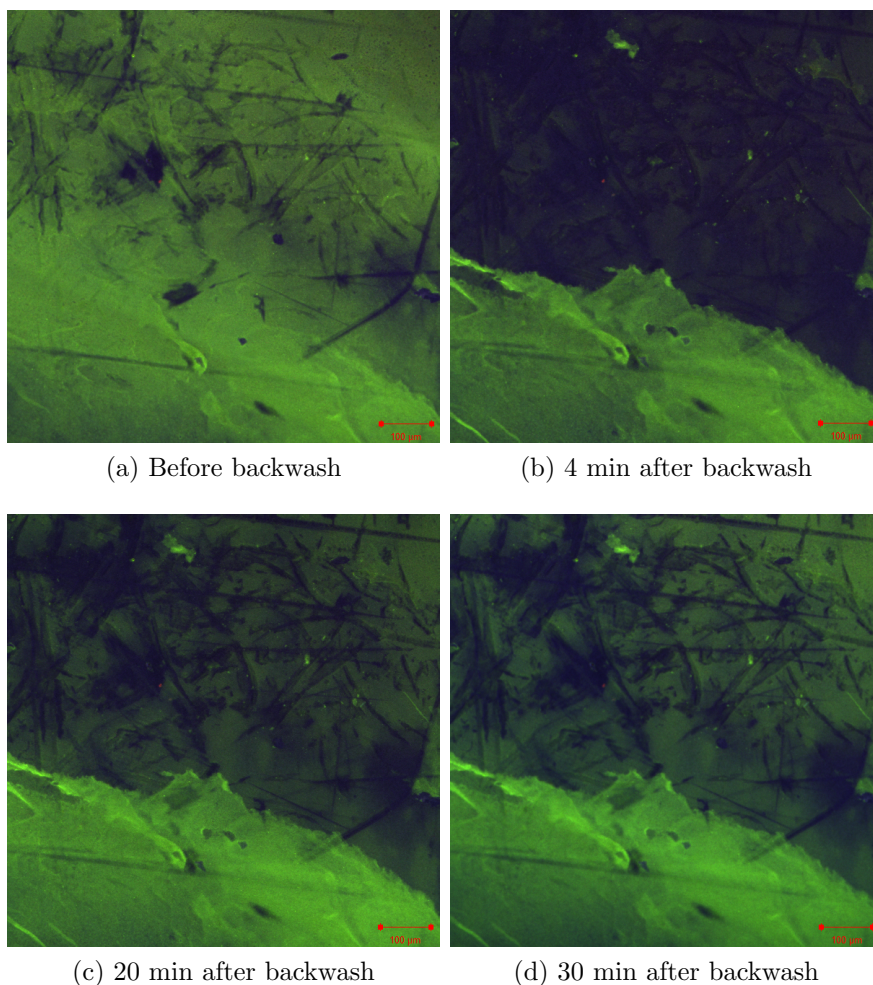
(c) 20 min after backwash

(d) 30 min after backwash

Figure 13: Confocal images of the progression of UF membrane fouling after a backwash. All images are collected after 3 d of fouling and the time since the last backwash is specified below each image. Region A is also depicted in Fig. 14 and Region B is also depicted in Fig. 15. Blue = DAPI; green = EPS (WGA); red = dead cells (PI).

in large (>100 µm) flakes with well-defined edges and leaves large areas of membrane nearly clean, but has little effect on other membrane regions. The effect of backwashing is captured in more detail in Figs. 14 and 15, which highlight smaller regions of the membrane at several different times. While large regions of the membrane are left almost clean (see, e.g., Fig. 15), other areas in each image show no change and seem to be unaffected by backwashing. Some sections of foulant move in the direction of flow but stay attached to the membrane (compare Figs. 15c and d). Some regions even accumulate more foulant as sheets that peeled

27

off elsewhere pile up on the membrane (see, e.g., Fig. 14d). The thicker regions of layered or wrinkled foulant are evident in a 3-D rendering of the biofilm (Fig. 15c). Repeated disruption by backwashing also makes the biofilm accumulate unevenly over time, as demonstrated by the nonlinear progression of average biofilm thickness (see captions of Fig. 14) over time (computed as described in Sec. 2.6 from 3-D images taken prior backwashing at the same location shown).

In a separate experiment to observe the backwashing process itself, a UF membrane was fouled with periodic backwashes for 2 d. A cohesive film formed, as shown in Fig. 16a. During the backwash process, images showed the film detaching from the membrane in several places and ballooning into a bubble wrap–like structure (Fig. 16b); in the imaging plane of the 3-D structure, the cross-section of the biofilm appears as a set of closed forms. (For reference, both 2-D and 3-D images of a similar structure are shown in Fig. 17.) As seen in Fig. 16c, this backwash was ultimately not successful at removing the film, and the film appears largely unchanged after backwashing but for a slight change in the shape of large the wrinkle near the middle of the image.

The ineffectiveness of the backwash shown in Fig. 16 and the removal of foulant in large flakes in the more successful backwashes shown earlier (e.g., Fig. 14) demonstrates the cohesiveness of the biofilms formed on the UF membrane and provide some insight into biofouling mitigation strategies. Removal of organic foulant from RO and FO membranes in large flakes and sheets was previously demonstrated [9, 8]. Furthermore, the dark lines on the membrane that never seem to accumulate foulant often coincide with the edges of patches where flakes are removed during backwashing. A similar pattern is also seen in SEM image of the unfouled UF membrane (Fig. C.26), suggesting the membrane texture defines the placement of these low-fouling areas. We hypothesize that the edges of the thinner regions of biofilm that form over less-permeable membrane regions are more likely to tear and allow for the removal of flakes. Intentionally patterning membranes with low-permeability regions

28

(a) 2 d, pre-BW, 10.0 µm thick

(b) 2 d, post-BW

(c) 3 d, pre-BW, 35.4 µm thick

(d) 3 d, post-BW

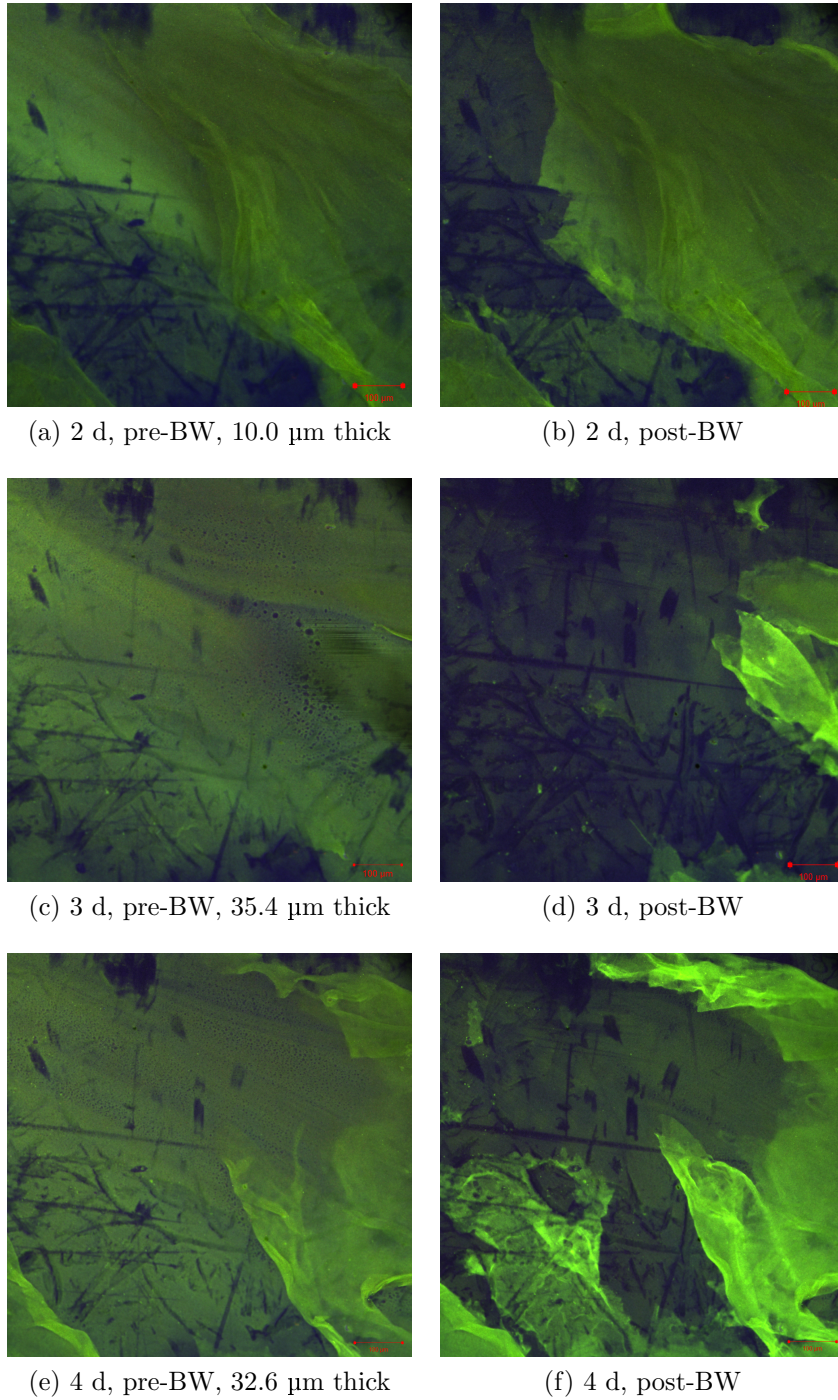(e) 4 d, pre-BW, 32.6 µm thick

(f) 4 d, post-BW

Figure 14: Confocal images of a single region of fouled UF membrane captured in situ with a 10x objective before and after a backwash (BW). Blue = DAPI; green = EPS (WGA); red = dead cells (PI). Average biofilm thicknesses before backwash, calculated from 3-D images, are included in sub-figure captions to show nonlinear biofilm accumulation.
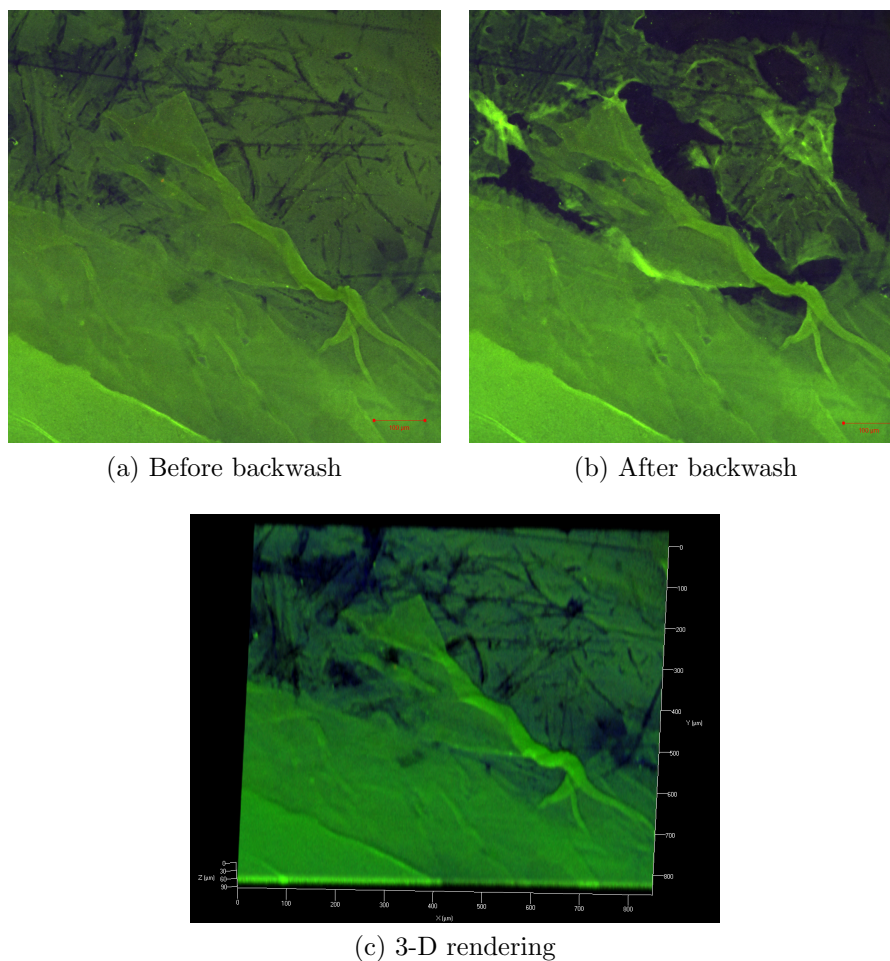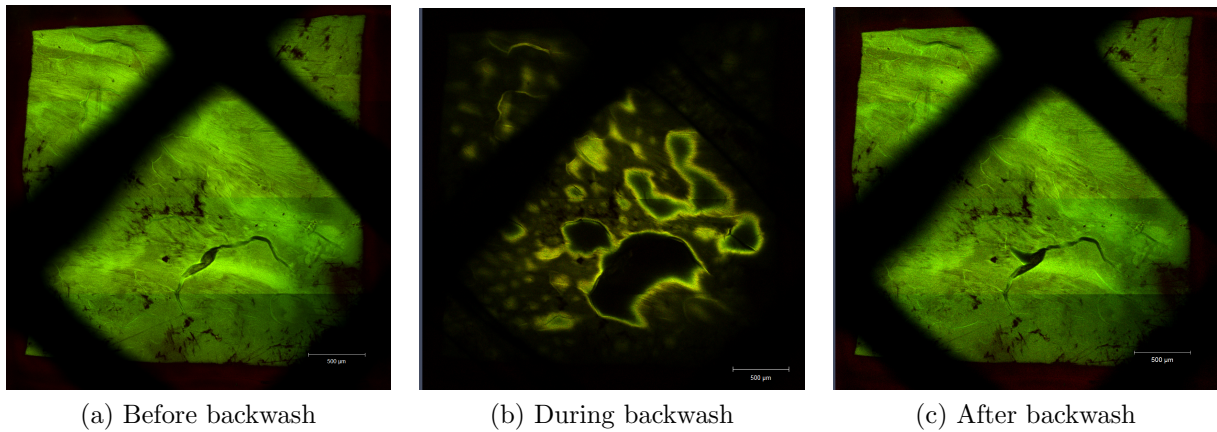
(a) Before backwash

(b) After backwash

(c) 3-D rendering

Figure 15: Confocal images of a single region of fouled UF membrane after 4 d, captured in situ with a 10x objective. Blue = cells (DAPI); green = EPS (WGA); red = dead cells (PI).

could be a method of raising the effectiveness of backwashing with the potential outcome of raising the flux at which the membrane can be operated long-term or extending the time between chemical cleans.

3.5. Discussion

3.5.1. In situ vs. ex situ imaging

This study was carried out to better understand fouling progression as well as to separate realistic membrane biofouling behaviors from artefacts of ex situ imaging. As shown in Fig. 17, sample removal and simple preparation for imaging (placing on a slide in a drop of feed

(a) Before backwash   (b) During backwash   (c) After backwash

Figure 16: Confocal images of a single region of 2-day fouled UF membrane captured in situ with a 10x objective (a) before, (b) during, and (c) after an ineffective backwash. Green = EPS (WGA); red = dead cells (PI). Scale bars (lower right of each image) span 500 µm.

liquid under a coverslip) caused a rapid (<30 min) change in foulant conformation from flat to buckled; in this case, a 2-D slice and 3-D rendering of the biofilm imaged ex situ show delamination of the biofilm from the MF membrane in a pattern reminiscent of bubble wrap. The in situ and ex situ images in Fig. 17 do not correspond to the same location on the membrane, but the in situ image of the entire membrane (Fig. 3) shows that bubble wrap-like delamination did not occur anywhere on the membrane during filtration.

Similar buckled conformations have been observed in ex situ CLSM images of membrane-bound biofilms previously [17, 31]. In the present study, cleaning processes involving relaxation (see Appendix B.1) and salinity change (see Appendix B.2) created similar conformations in the biofilm in situ. Bar-Zeev et al. [31] noticed a similar buckled conformation in ex situ imaging of biofilms, including changes in biofilm conformation when a glass coverslip was placed on a hydrated biofilm for ex situ imaging. They attributed the flatter conformation under the coverslip to a change (flattening) induced by the coverslip; however, without in situ imaging, the original biofilm conformation before removal from the operating conditions of the flow cell cannot be known.

Biofilm delamination from the membrane during preparation for ex situ imaging may

31

(a) In situ
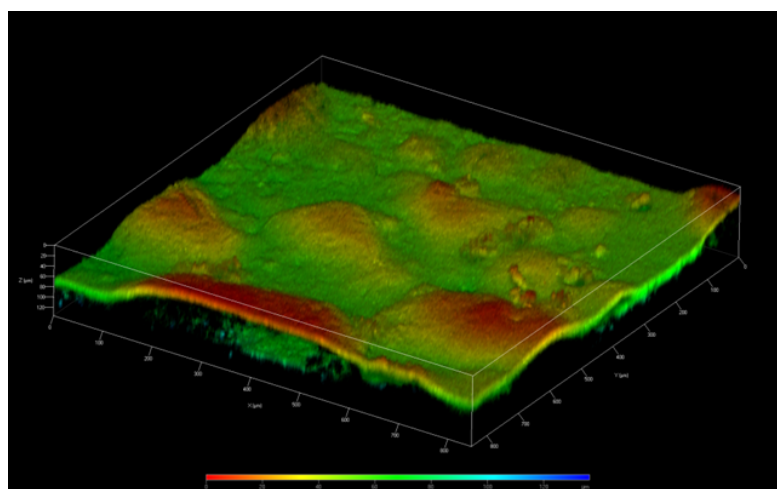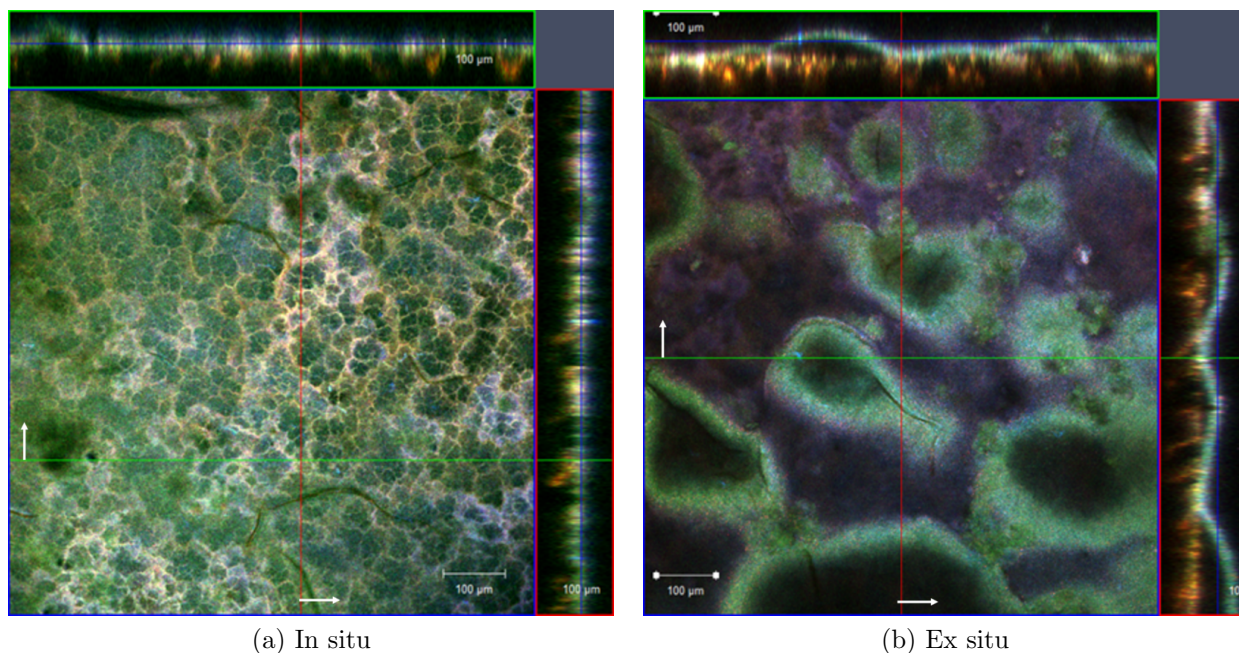

(b) Ex situ

(c) Ex situ: 3-D rendering

Figure 17: In situ and ex situ images of a 4 day-old MF biofilm. (a) shows the biofilm is initially flat, but image (b) (and its rendering in (c)) of a region of the biofilm shortly after removal from the flow cell demonstrates buckling into a characteristic bubble wrap–like conformation. Cyan = cells (Hoechst); green = EPS (WGA); red = dead cells (PI). Depth section planes are indicated with arrows.

494 occur due to changes in nutrient availability when cross-flow and transmembrane flux no

495 longer bring sufficient nutrients to the biofilm. Hunt et al. [45] observed that *P. aeruginosa*

496 biofilms detached from a stainless steel substrate both under stagnation conditions (when

flow was stopped) or when the flowing solution was replaced with a nutrient-scarce solution. A biofilm grown on a membrane under particular conditions may begin to detach when conditions change in preparation for ex situ imaging. As shown in Fig. 17, the remarkable change in the membrane-grown biofilm upon removal from filtration conditions demonstrates the limitations of ex situ imaging and the importance of not only in situ but *operando* imaging for understanding the conformations and behaviors of membrane biofouling.

3.5.2. Fouling behaviors and mechanisms

Several accumulation and removal behaviors were revealed through in situ imaging of wastewater effluent filtration with periodic backwashing. UF membrane images in Fig. 18 highlight regions where foulant advection, sloughing, and accumulation are significant. In parts of the membrane that were successfully cleaned by a recent backwash, high flux through the clean membrane brings new biofilm components to the surface. In parts of the membrane where local permeation is low due to membrane damage or prior biofouling, additional foulant accumulation occurs slowly or not at all. During a backwash, part of the membrane is cleaned, while other sections remain covered in biofilm; some regions even accumulate additional fouling during the backwashing process if the delaminated biofilm folds or re-deposits elsewhere. MF displayed similar accumulation and removal behaviors and additionally exhibited internal fouling with significant EPS accumulation inside large internal pores, as shown in Fig. 6.

Biofouling behaviors on membranes with permeation, cross-flow, and periodic backwashing are shaped by a variety of mechanisms. Observed behaviors are qualitatively arrayed, using micrographs from this report, from biologically- to physically-mediated in Fig. 19 to illustrate the range of filtration membrane biofouling behaviors observed in this study. Better understanding of membrane biofouling through in situ visualization enables insight into potential improvements to membranes and processes in water reuse applications, such as patterning membranes to encourage biofilm flake sloughing, as discussed in Sec. 3.4.
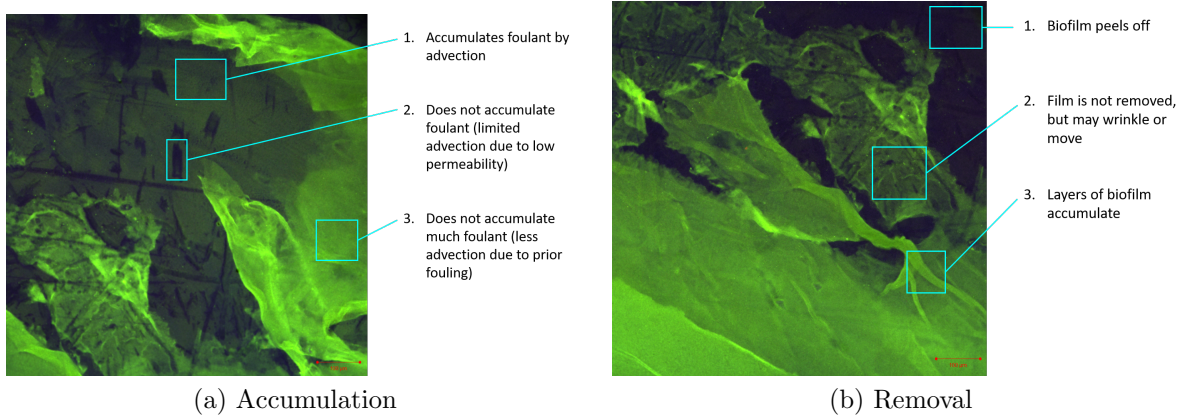
(a) Accumulation

1. Accumulates foulant by advection
2. Does not accumulate foulant (limited advection due to low permeability)
3. Does not accumulate much foulant (less advection due to prior fouling)

(b) Removal

1. Biofilm peels off
2. Film is not removed, but may wrinkle or move
3. Layers of biofilm accumulate

Figure 18: Summary of accumulation and removal behaviors in ultrafiltration with periodic backwash

Biological ⟷ Physical

Reproduction   Patterning   Tearing   Convection

EPS production   Internal fouling   Delamination   Re-deposition
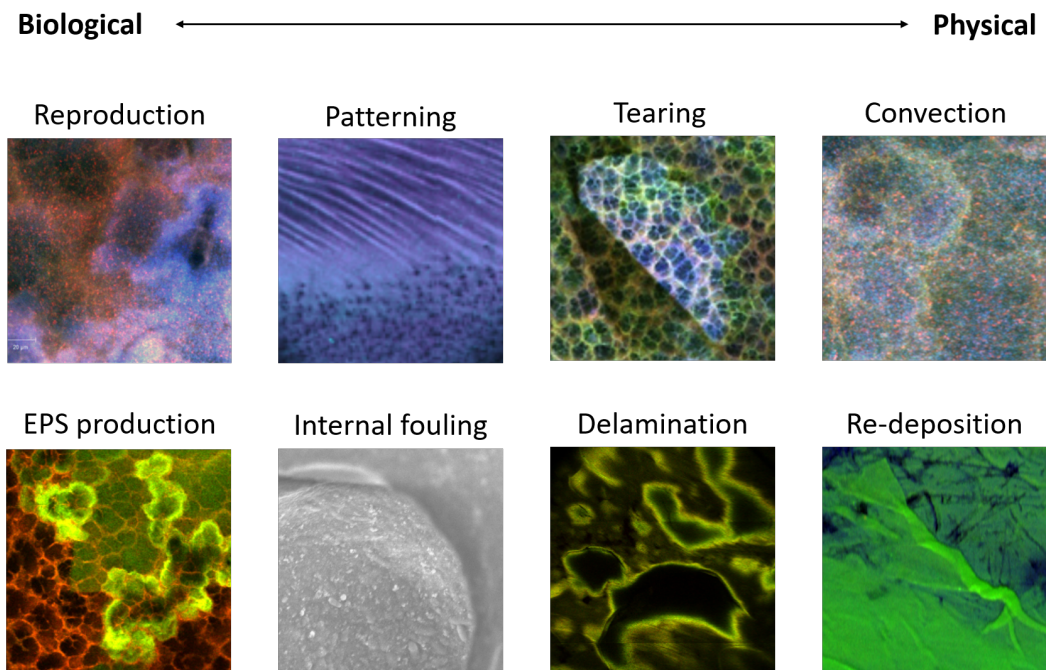
Figure 19: Graphical summary of biofouling behaviors observed throughout this study

3.5.3. Limitations

We acknowledge several limitations of this study's method of visualizing biofouling mechanisms in water reuse. The longest experiments, at 4 d in duration, were still significantly shorter than the multi-year lifespan of an MF or UF membrane, so long-term fouling be-

haviors were not captured by this study. The experimental apparatus also used a relatively low flux for backwashing and did not incorporate air scouring, which is an aspect of backwash procedures in reuse facilities [33]. The persistent use of stains, especially live cell stains (see Appendix A), had an unknown effect on the behavior of the biofilm-forming microbes; similarly, the unrealistically long feedwater storage times prior to filtration (days to weeks) had an unknown effect on fouling behavior. While the small imaging area was large enough to observe heterogeneity in fouling behavior on the scale of a feed spacer cell, it was far too small to capture variations that might exist between distant parts of a commercial membrane element. Finally, the thin glass slide used to seal the flow cell and allow imaging was both too thin to allow application of the high pressures used in RO, another biofouling-prone membrane process common in potable water reuse, and too thick to allow for CLSM imaging at the resolution required to visualize the biofilm conformation at the level of individual cells due to the short working distances associated with high-resolution objectives. While these limitations prevented visualization of the exact behavior of real wastewater reuse biofilms, the use of realistic hydrodynamic conditions and real wastewater effluent provide some insight into biofouling behaviors that can only be observed in situ.

Future work might mitigate several of the aforementioned limitations by improving the flow cell design. Using hollow fiber membranes could allow for both plane views and cross-sectional views of the biofilm, despite the poor vertical resolution of the long working distance objectives; hollow fiber membranes are also more realistic in MF and UF for water reuse. Designing a flow cell into which a water immersion objective could be integrated would also improve resolution and enable quantitative analysis of biofilm characteristics such as porosity. Using new ultra-permeable RO membranes could enable in situ visualization of RO membrane fouling with UF/MF permeate at relatively low pressures, although dye rejection by the membranes would be a concern that would need to be mitigated, perhaps by replacement of the wastewater effluent shortly after introducing stains.

35

4. Conclusion

In situ confocal laser scanning microscopy of membrane biofilms under filtration conditions was used to elucidate biofouling behaviors in MF and UF. Biofilms formed within minutes due to convection of water constituents to the membranes at high flux, causing external fouling of both MF and UF membranes. Additionally, in situ CLSM and ex situ SEM images showed that MF membranes exhibited internal fouling, with apparent cell proliferation and EPS production within networks of large pores beneath the membrane surface.

Biofouling behavior in conditions with periodic backwashing was influenced by the cohesiveness that is a hallmark of biofilms. Behaviors including wrinkling, delamination, tearing, and re-deposition after backwashes were influenced by the mechanics of the biofilm, including its cohesion and its adhesion to the membrane. Buckling of the biofilm in a characteristic bubble wrap-like conformation was observed during backwashing, relaxation, and high-salinity soaking as well as after removal from the flow cell for ex situ imaging. Patterning of the biofilm at the scale of 10–50 microns was also observed, rendering visible the complex interplay of microbiology, local hydrodynamics, mechanics, and mass transfer that dictates biofouling behavior.

Observed changes in biofilm conformation between in situ and ex situ CLSM images highlight the importance of in situ and *operando* imaging for understanding biofouling behavior, particularly when biofilm conformation is of interest. Biofilm delamination was observed even during in situ imaging under relaxation conditions (i.e., no flux or cross-flow), indicating the responsiveness of the biofilm to subtle changes in its environment. While promising in situ imaging methods continue to be developed, we invite fouling researchers to recognize the possibility of rapid conformational change when biofilms are removed from filtration conditions for ex situ imaging.

36

Acknowledgments

CRediT authorship statement

EWT: Conceptualization, methodology, investigation, data curation, formal analysis, resources, writing—original draft, writing—review and editing, visualization, funding acquisition. BR: Methodology, formal analysis, resources, writing—review and editing. RK: supervision, writing—review and editing, funding acquisition.

References

[1] A. Sim, M. S. Mauter, Cost and energy intensity of US potable water reuse systems, Environmental Science: Water Research & Technology (2021).

[2] D. M. Warsinger, S. Chakraborty, E. W. Tow, M. H. Plumlee, C. Bellona, S. Loutatidou, L. Karimi, A. M. Mikelonis, A. Achilli, A. Ghassemi, L. P. Padhye, S. A. Snyder, S. Curcio, C. D. Vecitis, H. A. Arafat, J. H. Lienhard, A review of polymeric membranes and processes for potable water reuse, Progress in Polymer Science 81 (2018) 209–237.

[3] D. Potts, R. C. Ahlert, S. S. Wang, A critical review of fouling of reverse osmosis membranes, Desalination 36 (1981) 235–264.

[4] Q. She, R. Wang, A. G. Fane, C. Y. Tang, Membrane fouling in osmotically driven membrane processes: A review, Journal of Membrane Science 499 (2016) 201–233.

[5] M. T. Khan, M. Busch, V. G. Molina, A.-H. Emwas, C. Aubry, J.-P. Croue, How different is the composition of the fouling layer of wastewater reuse and seawater desalination RO membranes?, Water Research 59 (2014) 271 – 282.

[6] M. Luo, Z. Wang, Complex fouling and cleaning-in-place of a reverse osmosis desalination system, Desalination 141 (2001) 15–22.

[7] W. G. Characklis, Bioengineering report: Fouling biofilm development: A process analysis, Biotechnology and Bioengineering 23 (1981) 1923–1960.

[8] G. S. Goon, O. Labban, Z. H. Foo, X. Zhao, J. H. Lienhard, Deformation-induced cleaning of organically fouled membranes: Fundamentals and techno-economic assessment for spiral-wound membranes, Journal of Membrane Science 626 (2021) 119169.

[9] E. W. Tow, M. M. Rencken, J. H. Lienhard V, In situ visualization of organic fouling and cleaning mechanisms in reverse osmosis and forward osmosis, Desalination 399 (2016) 138–147.

[10] L. Fortunato, S. Jeong, T. Leiknes, Time-resolved monitoring of biofouling development on a flat sheet membrane using optical coherence tomography, Scientific Reports 7 (2017) 15.

[11] L. Fortunato, S. Bucs, R. V. Linares, C. Cali, J. S. Vrouwenvelder, T. Leiknes, Spatially-resolved in-situ quantification of biofouling using optical coherence tomography (OCT) and 3D image analysis in a spacer filled channel, Journal of Membrane Science 524 (2017) 673 – 681.

[12] L. Fortunato, T. Leiknes, In-situ biofouling assessment in spacer filled channels using optical coherence tomography (OCT): 3D biofilm thickness mapping, Bioresource Technology 229 (2017) 231–235.

[13] A new high-pressure optical membrane module for direct observation of seawater ro membrane fouling and cleaning, Journal of Membrane Science 364 (2010) 149–156.

[14] D. Hughes, U. K. Tirlapur, R. Field, Z. Cui, In situ 3D characterization of membrane fouling by yeast suspensions using two-photon femtosecond near infrared non-linear optical imaging, Journal of Membrane Science 280 (2006) 124–133.

[15] S.-T. Kang, A. Subramani, E. M. Hoek, M. A. Deshusses, M. R. Matsumoto, Direct observation of biofouling in cross-flow microfiltration: mechanisms of deposition and release, Journal of Membrane Science 244 (2004) 151–165.

[16] N. Farhat, J. Vrouwenvelder, M. Van Loosdrecht, S. Bucs, M. Staal, Effect of water temperature on biofouling development in reverse osmosis membrane systems, Water Research 103 (2016) 149–159.

[17] S. E. Kwan, E. Bar-Zeev, M. Elimelech, Biofouling in forward osmosis and reverse osmosis: Measurements and mechanisms, Journal of Membrane Science 493 (2015) 703–708.

38

[18] R. J. Palmer, J. A. J. Haagensen, T. R. Neu, C. Sternberg, Handbook of Biological Confocal Microscopy, Springer US, Boston, MA, pp. 870–888.

[19] T. R. Neu, J. R. Lawrence, Investigation of Microbial Biofilm Structure by Laser Scanning Microscopy, Springer International Publishing, pp. 1–51.

[20] A. Bridier, F. Dubois-Brissonnet, A. Boubetra, V. Thomas, R. Briandet, The biofilm architecture of sixty opportunistic pathogens deciphered using a high throughput CLSM method, Journal of Microbiological Methods 82 (2010) 64 – 70.

[21] M. Alhede, K. Qvortrup, R. Liebrechts, N. Høiby, M. Givskov, T. Bjarnsholt, Combination of microscopic techniques reveals a comprehensive visual impression of biofilm structure and composition, FEMS Immunology & Medical Microbiology 65 (2012) 335–342.

[22] J. R. Lawrence, G. D. W. Swerhone, G. G. Leppard, T. Araki, X. Zhang, M. M. West, A. P. Hitchcock, Scanning transmission x-ray, laser scanning, and transmission electron microscopy mapping of the exopolymeric matrix of microbial biofilms, Applied and Environmental Microbiology 69 (2003) 5543–5554.

[23] M. Wagner, N. P. Ivleva, C. Haisch, R. Niessner, H. Horn, Combined use of confocal laser scanning microscopy (CLSM) and raman microscopy (RM): Investigations on EPS - matrix, Water Research 43 (2009) 63 – 76.

[24] H.-C. Flemming, The Perfect Slime: Microbial Extracellular Polymeric Substances (EPS), IWA publishing, pp. 1–14.

[25] M. Klausen, A. Aaes-Jørgensen, S. Molin, T. Tolker-Nielsen, Involvement of bacterial migration in the development of complex multicellular structures in Pseudomonas aeruginosa biofilms, Molecular Microbiology 50 (2003) 61–68.

[26] T. Thurnheer, R. Gmür, B. Guggenheim, Multiplex fish analysis of a six-species bacterial biofilm, Journal of Microbiological Methods 56 (2004) 37–47.

[27] W. Manz, K. Wendt-Potthoff, T. Neu, U. Szewzyk, J. Lawrence, Phylogenetic composition, spatial structure, and dynamics of lotic bacterial biofilms investigated by fluorescent in situ hybridization and confocal laser scanning microscopy, Microbial Ecology 37 (1999) 225–237.

[28] C. Staudt, H. Horn, D. C. Hempel, T. R. Neu, Volumetric measurements of bacterial cells and extracellular polymeric substance glycoconjugates in biofilms, Biotechnology and Bioengineering 88 (2004) 585–592.

[29] E. L. Farias, K. J. Howe, B. M. Thomson, Spatial and temporal evolution of organic foulant layers on

reverse osmosis membranes in wastewater reuse applications, Water Research 58 (2014) 102 – 110.

[30] A. Kastl, A. Bogler, M. Spinnler, T. Sattelmayer, A. Be'er, E. Bar-Zeev, Impact of hydrodynamics on the first stages of biofilm formation in forward osmosis with spacers, Environmental Science & Technology 54 (2020) 5279–5287.

[31] E. Bar-Zeev, K. R. Zodrow, S. E. Kwan, M. Elimelech, The importance of microscopic characterization of membrane biofilms in an unconfined environment, Desalination 348 (2014) 8–15.

[32] A. Manti, P. Boi, T. Falcioni, B. Canonico, A. Ventura, D. Sisti, A. Pianetti, M. Balsamo, S. Papa, Bacterial cell monitoring in wastewater treatment plants by flow cytometry, Water Environment Research 80 (2008) 346–354.

[33] J. Wong et al., Membrane Applications for Water Reuse, Technical Report, American Water Works Association, 2018.

[34] Wheat Germ Agglutinin Conjugates, Invitrogen, 2009 [Online].

[35] T. R. Neu, U. Kuhlicke, Fluorescence lectin bar-coding of glycoconjugates in the extracellular matrix of biofilm and bioaggregate forming microorganisms, Microorganisms 5 (2017) 5.

[36] Propidium Iodide Nucleic Acid Stain, Invitrogen, 2006 [Online].

[37] Hoechst Stains, Invitrogen, 2005 [Online].

[38] DAPI Nucleic Acid Stain, Invitrogen, 2006 [Online].

[39] R. E. Durand, P. L. Olive, Cytotoxicity, mutagenicity and DNA damage by Hoechst 33342., Journal of Histochemistry & Cytochemistry 30 (1982) 111–116.

[40] D. McDougald, N. Barraud, P. D. Steinberg, S. A. Rice, S. Kjelleberg, Should we stay or should we go: mechanisms and ecological consequences for biofilm dispersal, Nature Reviews Microbiology 10 (2012) 39.

[41] J. S. Webb, L. S. Thompson, S. James, T. Charlton, T. Tolker-Nielsen, B. Koch, M. Givskov, S. Kjelleberg, Cell death in pseudomonas aeruginosa biofilm development, Journal of Bacteriology 185 (2003) 4585–4592.

[42] E. Bar-Zeev, M. Elimelech, Reverse osmosis biofilm dispersal by osmotic back-flushing: Cleaning via substratum perforation, Environmental Science & Technology Letters 1 (2014) 162–166.

[43] P. S. Stewart, Mini-review: Convection around biofilms, Biofouling 28 (2012) 187–198.

[44] L. E. P. Dietrich, C. Okegbe, A. Price-Whelan, H. Sakhtah, R. C. Hunter, D. K. Newman, Bacterial community morphogenesis is intimately linked to the intracellular redox state, Journal of Bacteriology 195 (2013) 1371–1380.

[45] S. M. Hunt, E. M. Werner, B. Huang, M. A. Hamilton, P. S. Stewart, Hypothesis for the role of nutrient starvation in biofilm detachment, Applied and Environmental Microbiology 70 (2004) 7418–7425.

[46] S. Lee, M. Elimelech, Salt cleaning of organic-fouled reverse osmosis membranes, Water Research 41 (2007) 1134–1142.

Appendix A. Effect of live cell stain

Due to the potential cytotoxicity and mutagenicity of Hoechst 33342 [39], an analogous experiment to that reported in Section 3.2 was conducted in which Hoechst was only added prior to the last imaging session to qualitatively determine the effect of frequent Hoechst application on the fouling behavior in the experiments reported on throughout this study. 2.9 µg/mL of WGA and 1.2 µg/mL of PI were added daily before imaging, and 1.8 µg/mL Hoechst was added just before the final imaging session after 4 d of fouling. MF membrane images with and without the daily application of Hoechst are compared in Fig. A.20. Both with and without Hoechst, after 4 d of fouling, a flat layer of live and dead cells and EPS forms on the active layer and internal fouling with live cells and EPS is apparent within large internal pores. The addition of Hoescht seems to dull the appearance of EPS whether it is added daily or just before the final imaging session. Without Hoechst, it is particularly apparent how concentrated EPS are at the edges of internal pores in which fouling occurs. The similarity of the biofilm at 4 d with and without daily application of Hoechst suggests that the daily use of Hoechst as reported on in Sec. 3 did not significantly affect qualitative fouling behavior.

The membrane of Fig. A.20 that was only treated with Hoechst once at 4 d was depth-scanned in Fig. A.21, confirming that what appears to be internal fouling does occur below the membrane active layer.
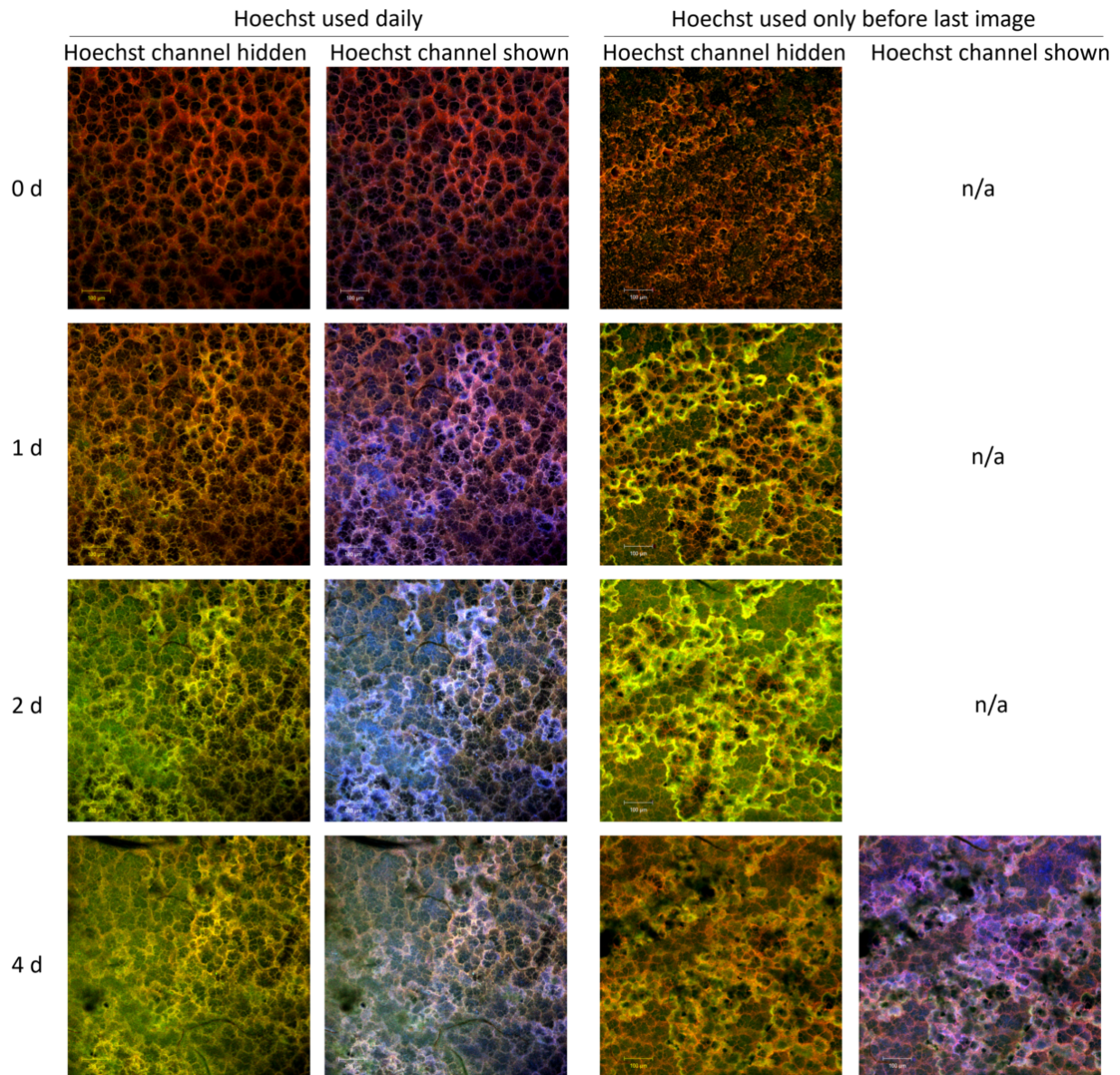
Figure A.20: Confocal images of fouled MF membrane with application of Hoechst daily and only just before the last imaging session, shown with and without the Hoechst channel illuminated. Blue = cells (Hoechst); green = EPS (WGA); red = dead cells (PI).

Appendix B. Additional cleaning procedures

Due to the cohesive external fouling observed on UF membranes, two cleaning procedures beyond backwashing were investigated. Anecdotal reports of relaxation-induced biofilm sloughing inspired the use of relaxation as a potential cleaning strategy, and past
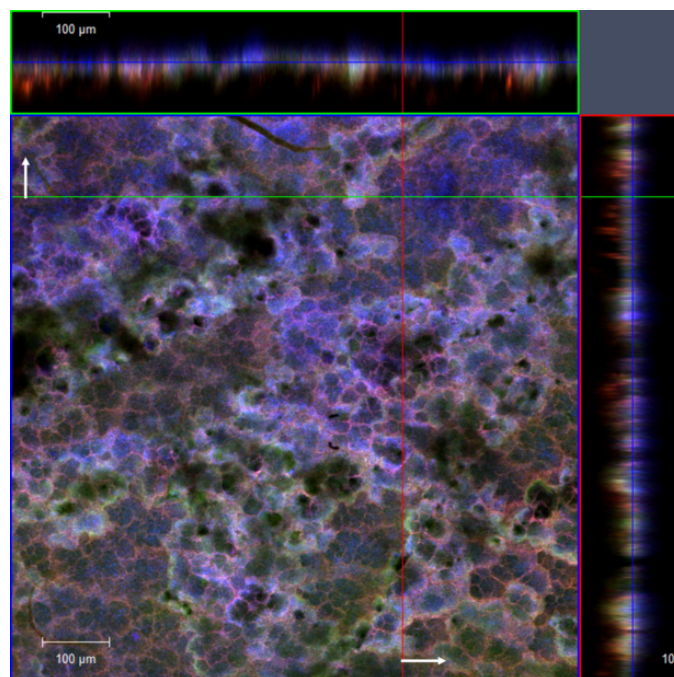
Figure A.21: 3-D scan of biofilm on MF membrane after 4 d with Hoechst added only before this final imaging session. Blue = cells (Hoechst); green = EPS (WGA); red = dead cells (PI). Depth section planes are indicated with arrows.

observation of effective organic fouling removal by salt cleaning [46] inspired the used of a saline soak. Neither strategy was effective as removing the biofilm, but both revealed biofilm delamination behavior, as discussed further below. Visualization of membrane cleaning with bleach was also attempted, but bleaching of the fluorescent probes occurred and the resulting images were not interpretable.

Appendix B.1. Relaxation

The biofilm shown in Fig. 9 was allowed to relax in order to observe biofilm behavior during stoppage of flux and cross-flow. After approximately 3 h of fouling at 20 cm/s cross-flow and approximately 48 LMH flux, both circulation and syringe pumps were stopped. Flux declined as pressure wound down to atmospheric. After about five hours with both pumps off, the biofilm was imaged again (Fig. B.22), revealing slight delamination of the biofilm from the membrane in a pattern of mounds, approximately 100 μm wide and 20 μm

43

tall, and oriented similarly to the stripe pattern shown in Figs. 9 and 10. These wrinkles show some similarity to the bubble wrap pattern seen in a biofilm imaged ex situ (Fig. 17b,c). Relaxation, as performed here, was not effective in cleaning the membrane, but did cause delamination, which points to potential for biofilm removal.

(a)   (b)
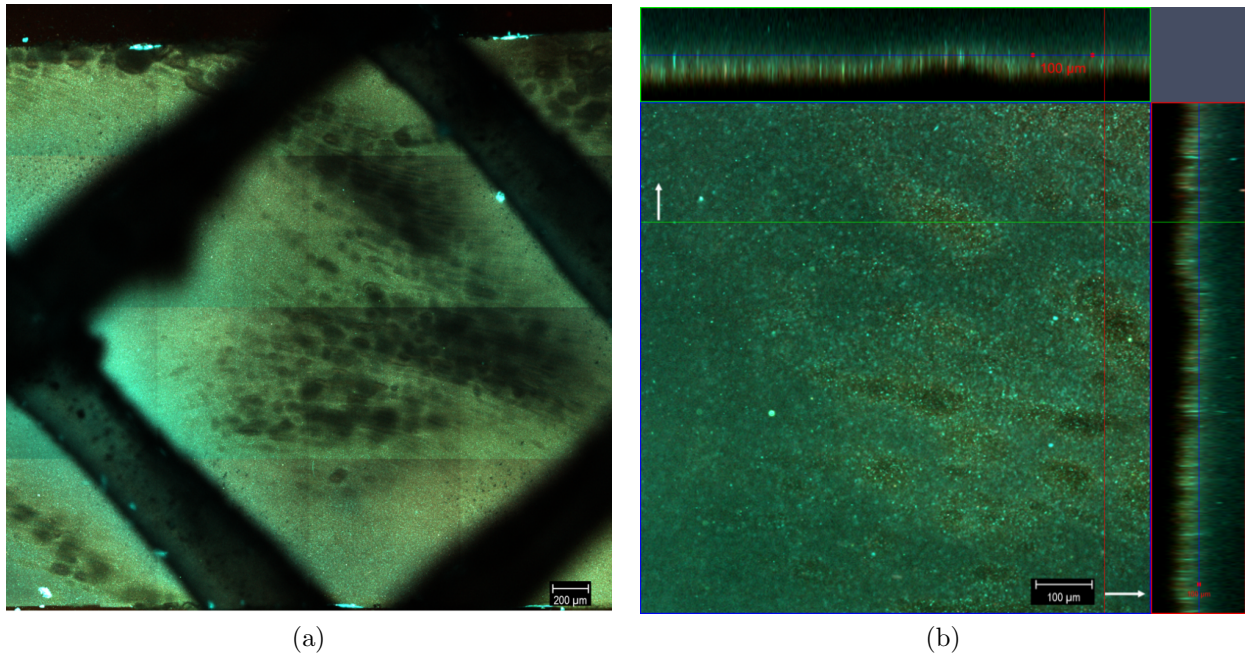
Figure B.22: 3-D wrinkling of UF biofilm after relaxation: (a) plane view and (b) close-up with cross-sectional views showing delamination. Cyan = cells (DAPI); green = EPS (WGA); red = dead cells (PI). Depth section planes are indicated with arrows.

Appendix B.2. Saline soak

A saline soak was used in an attempt to clean a UF membrane that had been fouled for 2 d with periodic backwashing. Shortly after a backwash that cleared part of the membrane, a 10% NaCl solution was introduced to the flow loop and the system was left to sit without cross-flow or applied pressure for approximately 30 min, during which time the membrane was imaged (Fig. B.23c), revealing delamination of sections of the remaining biofilm from the membrane. When cross-flow was restarted, the biofilm flattened again and was not removed. Although ineffective as a cleaning procedure, the finding of delamination during

44

a short saline soak (similar to behavior during a backwash, Fig. 16b, or a longer relaxation, Fig. B.22) is noteworthy.

(a) Before backwash

(b) After backwash

(c) During saline soak (8 min)

(d) After saline soak

Figure B.23: Backwashing and a saline soak were performed sequentially on a UF membrane fouled for 2 d. (a) and (b) show the effect of a backwash, while (c) and (d) show the effect of a saline soak.

Appendix C. SEM of clean and fouled membranes

Fouled MF membranes were examined with SEM (Ultra 55 FESEM, Carl Zeiss) to confirm suspected internal fouling.

To preserve the biofilm conformation, the fouled membrane was prepared for SEM as follows: Glutaraldehyde was added to the flow loop at a final concentration of 2.5% and left to fix cells for 30 min. The fouled membrane was removed from the cell and dipped for 10-15 min each in 10%, 25%, 75%, and 90% ethanol in deionized water and then twice in 100% ethanol to dehydrate the sample. The sample was finally vacuum dried and sputtered with gold using a SC7620 Mini Sputter Coater/Glow Discharge System (Electron Microscopy Sciences).

In SEM images of a fouled MF membrane (Fig. C.24), rod-shaped bacteria (bacilli) of approximately 2 µm length are seen lining a large internal pore that is visible through a hole in the surface; CLSM images in Section 3.2 suggest that such colonization of internal pores occurred throughout the membrane. Cracks in the fouled MF membrane are also visible, likely as a result of the drying process.

Unfouled MF and UF membranes were gold-sputtered and imaged with SEM to reveal membrane texture and aid interpretation of CLSM images. The MF membrane (Fig. C.25) displays large pores beneath the active layer, some of which connect to the active layer through holes that are large enough to allow bacteria to pass through. The UF membrane (Fig. C.26) has a smooth surface without visible pores at 168x magnification, but displays patterns that may have occurred in storage or handling. These membrane surface patterns appeared to affect fouling patterns, as shown in Section 3.4.
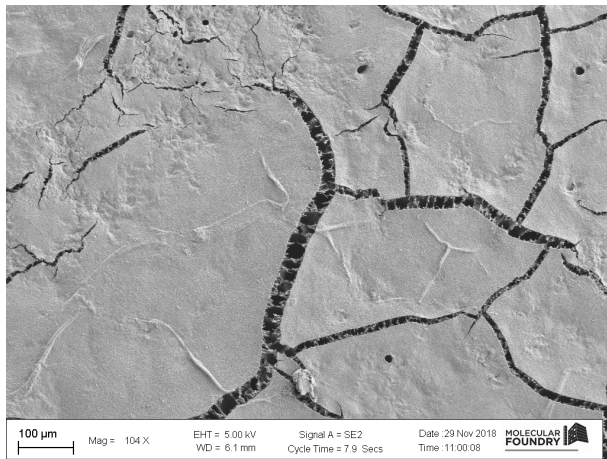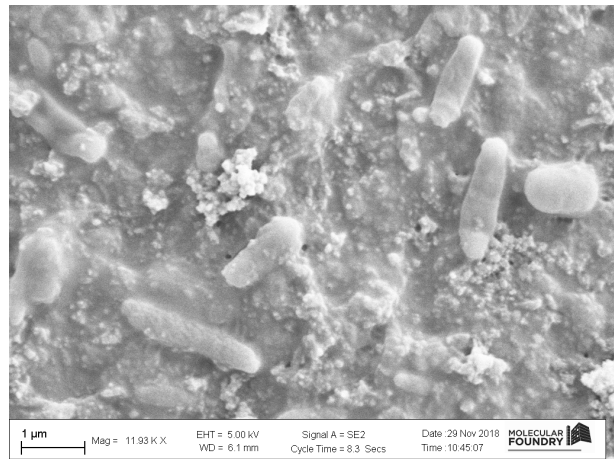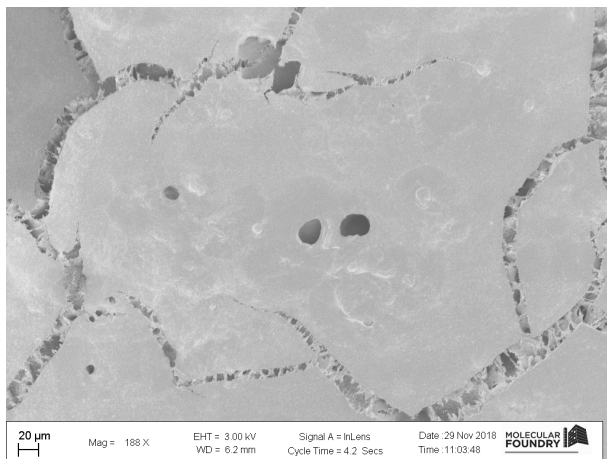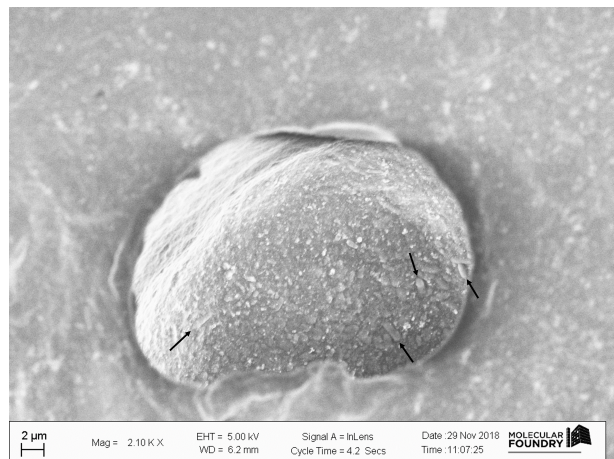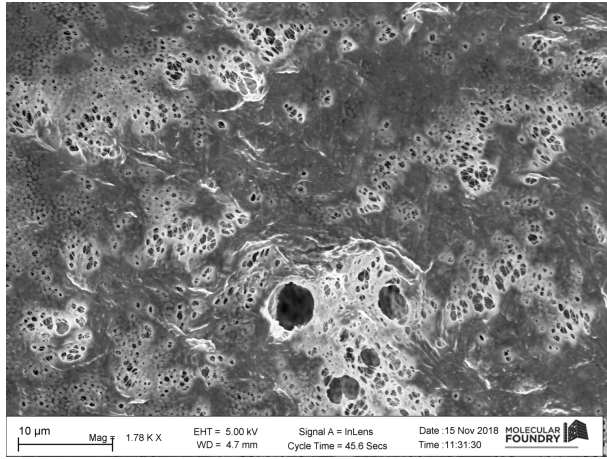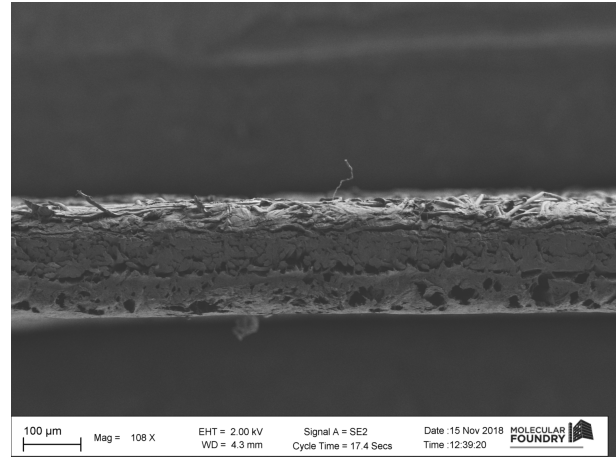
Figure C.24: SEM images of fouled MF membrane. (a) Wrinkles in the biofilm and cracks in the membrane surface. (b) Rod-shaped bacteria on the outer surface of the active layer. (c) Holes in the membrane and biofilm. (d) Rod-shaped bacteria inside one of the holes shown in (c) (several indicated with arrows; the reader may wish to zoom in; image contrast uniformly enhanced for visibility).
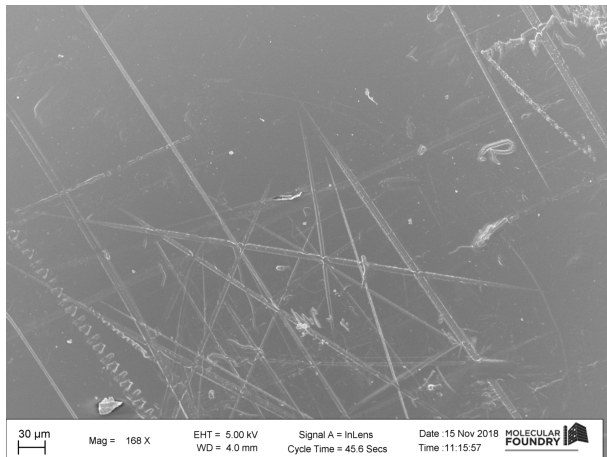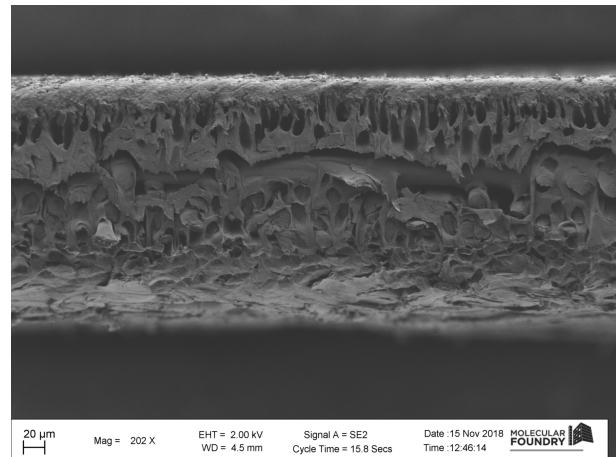
(a) Active layer

(b) Edge view (active layer facing down)

Figure C.25: SEM images of unfouled MF membrane (PVDF, Synder V0.1).

(a) Active layer

(b) Edge view (active layer facing up)

Figure C.26: SEM images of unfouled UF membrane (PES, Microdyn Nadir UP010).

Confocal laser scanning microscopy
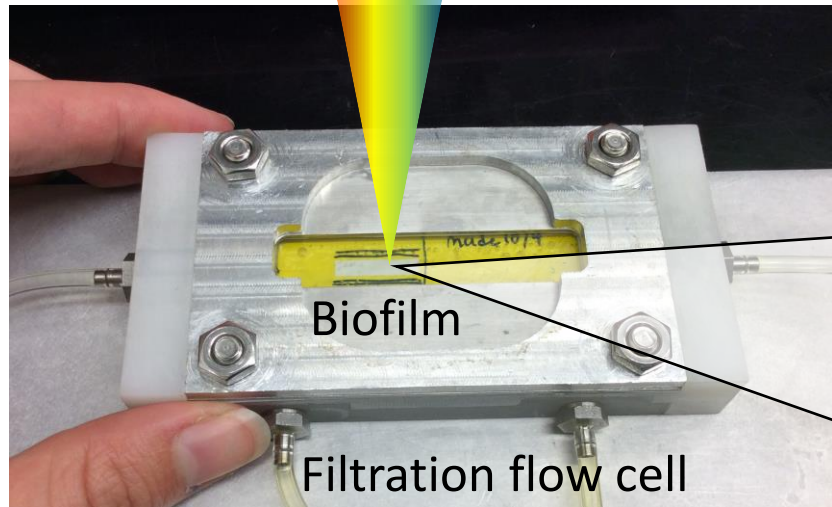
Biofilm

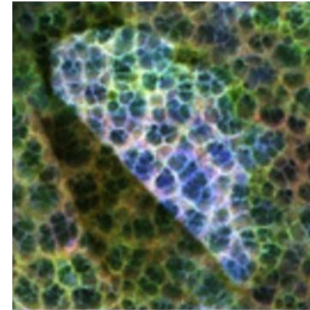Filtration flow cell

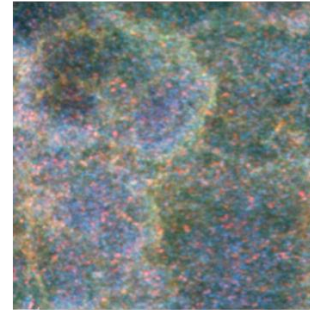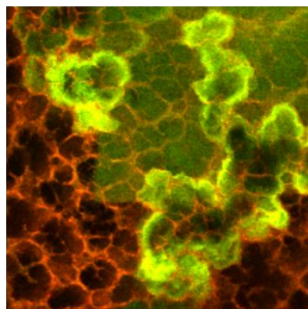**Biofouling mechanisms visualized in situ**
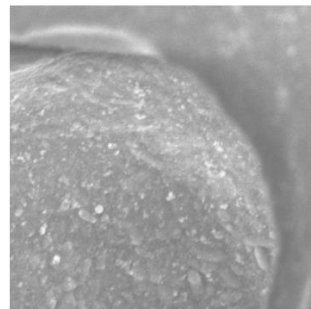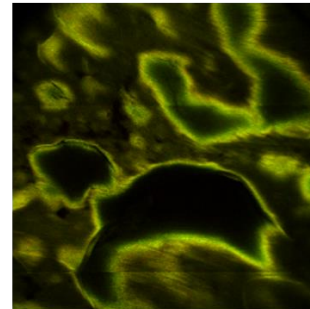
Reproduction

Patterning

Tearing

Convection

EPS production

Internal fouling

Delamination

Re-deposition